TOWARDS THE PRODUCTION OF NANOPARTICLES USING ENGINEERED PROTEIN SCAFFOLDS

By

JFM Bogers

to obtain the degree of Bachelor of Science
at the Delft University of Technology,
to be defended publicly on Friday July 14, 2017 at 10:00 AM.

Student number: 4252594
Program: BSc Nanobiology
Supervisor: Dr. G.E. Bokinsky
Daily supervisor: H. Shomar Monges, MSc

ABSTRACT

Metal nanoparticles have promising potential for use in medical applications, such as imaging or targeted drug delivery. Current methods of production of nanoparticles are expensive and make use of harsh reagents. Because of these limitations, nanoparticles are not yet widely available, limiting the use in medical applications. To commercialize nanoparticle production, it is necessary to develop a nanoparticle synthesis process that is cheap, safe and environmentally friendly. Earlier research has shown that biosynthesis of nanoparticles is possible in many different organisms using certain reducing peptide sequences. Biosynthesis of metallic nanoparticles is cheaper, safer and occurs under physiological conditions, making it an ideal process for the up scaling of nanoparticle production. However, shape and size of the nanoparticle are hard to control and yields are low when biosynthesis is used, limiting the use of biosynthesis. To overcome the problem of shape and size control, it is proposed to use viral capsids as protein cages to restrict the size of synthesized nanoparticles to the inside of the capsid. To implement this, metal ion reducing peptides were fused to the monomers of self-assembling capsids in a way that they were displayed on the inside of the capsid. It was shown that with the adjusted monomers, the capsids still self-assemble. Nanoparticle formation was attempted, but results were inconclusive.

TABLE OF CONTENTS

INTRODUCTION

NANOTECHNOLOGY

It all started back in 1959 with the physicist Richard Feynman and his talk "There's plenty of room at the bottom", which he held at a meeting for physicists. In this talk, he described how he wanted to control individual atoms and molecules and manipulate matter on an atomic scale (Feynman, 1957). This would involve using microscopes with the ability to detect and visualize objects at the nanoscale, which was not yet possible at that time. Feynmans talk did not gain much attention back then, but was later marked as the starting point of nanotechnology. Nanotechnology is defined as the understanding, control and restructuring of matter on the scale of 1 to 100 nm to create materials with fundamentally new properties and functions (NSTC, 2007). To give an idea of the scale nanotechnology operates in: you can compare a nano-sized particle to a football as the football to the earth.

With the development of the Scanning Tunneling Microscope (STM) and the Atomic Force Microscope (AFM) in the 1980's, visualization on the nanoscale became possible. The STM and AFM can image samples with very high precision and resolution, as they physically scan the surface of the sample and can detect height differences in the range of a few nanometer (Binnig & Rohrer, 1983) (Binnig & Quate, 1986). With these new techniques to visualize on the nanoscale, nanotechnology gained momentum. Nowadays nanotechnology is an established field, due to its contributions to a variety of fields. In medicine for instance, nanotechnology is used in diagnostics, drug delivery, tissue engineering and imaging. Nanotechnology is also heavily used in computers, gearing towards a quantum computer. Moreover nanotechnology can me employed to protect the environment, aiding the treatment of wastewater for example (Qu, Alvarez, & Li, 2013). In industry, nanotechnology is used for constructions of steel, glass, concrete (Sanchez & Sobolev, 2010) and coatings. Nanotechnology is also used for consumer products, such as food packaging (Duncan, 2014), optics, textiles, cosmetics and sports.

Nature is composed of nano-sized objects. DNA, for example, is a 2 nm think molecular helix found in every living cell. The aim to understand, manipulate, control or even engineer biomolecules and living organisms has boosted the biological applications of nanotechnology. Scientific research focused on biological and cellular nano-components, giving birth to an important branch of nanotechnology: nanobiology. Nanobiology deals with nanoscale biological interactions and also includes biological nanomachines and nanoparticles.

NANOPARTICLES

DEFINITION AND VARIETY

Nanoparticles are particles with a size between 1 and 100 nm in diameter. There are many different types of nanoparticles (figure I1) of varying composition, shape and size. Each type of nanoparticles holds unique properties that can be employed for specific applications. On one hand for example, liposomes, which are composed of a lipid bilayer, similar to cell membranes, can be used for drug delivery (Ostro & Cullis, 1989). On the other hand, metallic nanoparticles, mainly composed of noble metals, are more often used for medical diagnostics and nano optics (Kelly, Coronado, Zhao, & Schatz, 2003).

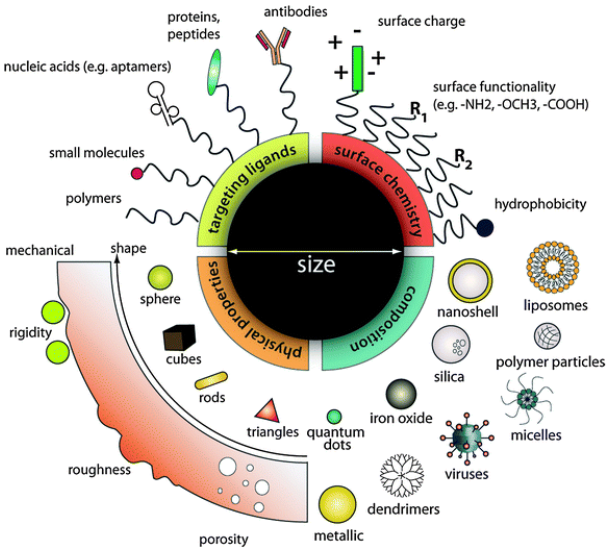

Figure I1: Variations is nanoparticle shape, size and material. (Chou, Ming, & Chan, 2011)

Metallic nanoparticles can be composed gold, silver, copper, lead, cobalt, zinc, nickel, platinum or even other metal alloys or metal oxides (extra reference 2). Nanoparticles come in various shapes, such as triangles, rods, cubes or spheres. The shape of the nanoparticle influences its properties in a similar way to the size (figure I2).

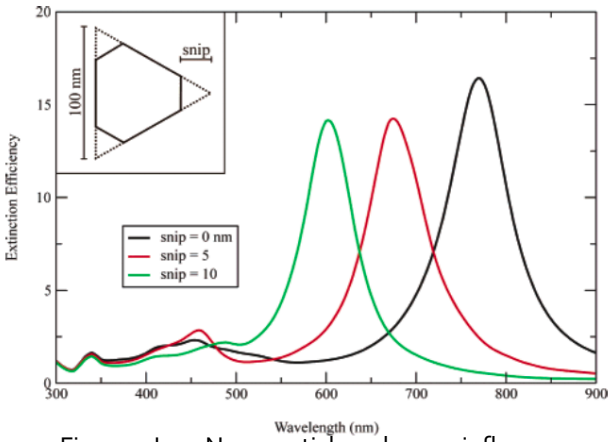

Figure I2: Nanoparticle shape influences wavelength of light absorbed. (Kelly et al., 2003)

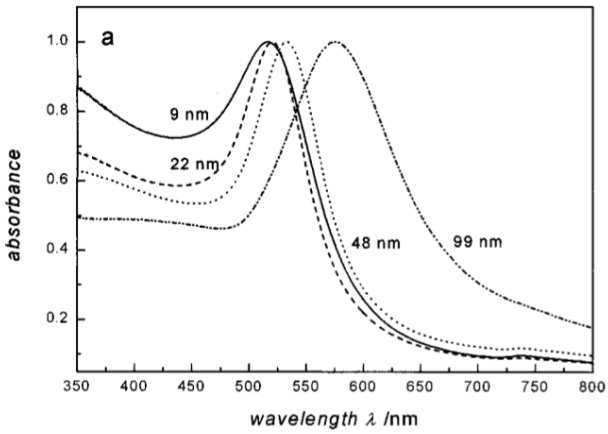

Figure I3: Nanoparticle size influences wavelength of light absorbed. (Link & El-Sayed, 1999)

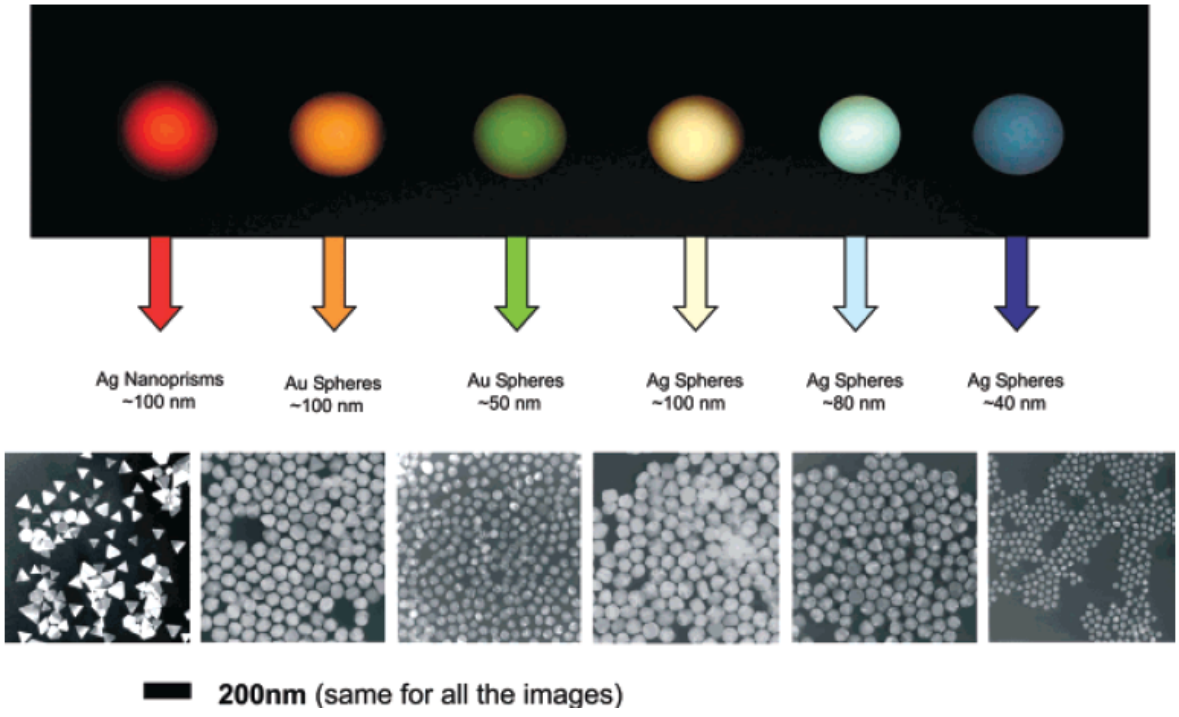

Figure I4: Nanoparticle size influences wavelength of light absorbed. (extra reference 6)

METAL NANOPARTICLES: PROPERTIES AND APPLICATIONS

While bulk materials exhibit constant physical properties, metal nanoparticles show size-dependent properties. As particles approach the nanoscale, the ratio between surface and volume of the particle becomes smaller, giving rise to remarkable properties (Akbari, Tavandashti, & Zandrahimi, 2011). Due to the large surface area when compared to volume, nanoparticles are effective catalysts (extra reference 3).

Moreover, metallic nanoparticles hold unique optical properties: the wavelength of absorbed light depends on the size of the nanoparticles in the solution (figure I3 and I4). This is caused by an effect called surface

plasmon resonance, which occurs when the size of the nanoparticle drops below the wavelength of light. Surface plasmon resonance consists of electron oscillations, excited by the electromagnetic field of light (Garcia, 2011). The electrons are restricted in their movement to the electromagnetic field of the light, emitting a different color from the bulk object of the same material. The noble metals silver, copper and gold show sharp peaks in the emission spectrum, while non-noble metals show a wide and less clear peak in the spectrum (Burda, Chen, Narayanan, & El-Sayed, 2005).

Diversity of biological applications and advantages

Metallic nanoparticles are used for various biological applications. For instance, silver nanoparticles display antibacterial properties that can be used in wound dressings (Said et al., 2014) and other related applications. Gold nanoparticles are used in microscope imaging or targeted drug delivery (Han, Ghosh, & Rotello, 2007). For example, in tumor targeting (for imaging or drug delivery purposes), nanoparticles are ideal to use. Because the nanoparticles are not able to leave the arteries in healthy tissue, as the particles are too big to exit trough the pores of the artery walls. But in the tumor, the pores in the artery walls are enlarged, as the tumor has pushed the formation of new arteries to the limit, making the formation sloppier. This enables the nanoparticles to exit the arteries at the tumor site and therefore targeting the tumor with high fidelity (Cho, Wang, Nie, Chen, & Shin, 2008).

Synthesis of metal nanoparticles

Current synthesis of metal nanoparticles and limitations

Currently metallic nanoparticles can be synthesized in many different ways, either chemically or physically. **Chemical methods include** (Dragomir, n.d.):

Chemical reduction of metal salts. Metal particles are formed when a solution is overly saturated with metal salts and under influence of a reducing agent. Because the solution is thermodynamically unstable, nucleation occurs, driving the solution in a more thermodynamically favorable state. After small particles are formed, they grow via addition of extra atoms.

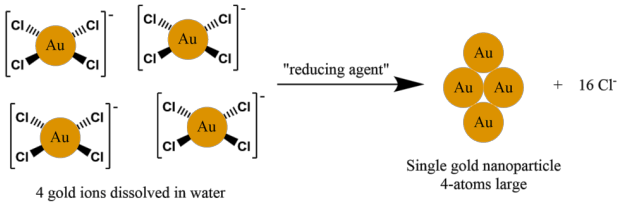

Figure I5: Chemical reduction of $AuCl_4^-$ into gold nanoparticles. (extra reference 7)

Microemulsions. Silver nanoparticles have shown to be formed using reverse micelles (Bae et al., 2005). Reverse micelles are used to contain small pools of water, in which silver salts were present. This causes a high concentration of silver salts, making nucleation more likely.

Thermal decomposition of metal salts

Electrochemical synthesis. This process makes use of an anode and a cathode. Metal ions are attracted towards the cathode; upon arrival, the ions are reduced and atoms are formed. The atoms aggregate in small particles, resulting in nanoparticles.

Physical methods include (Dragomir, n.d.):

- Exploding wire technique
- Plasma
- Chemical vapor deposition
- Microwave irradiation

- Pulsed laser ablation
- Supercritical fluids
- Sonochemical reduction
- Gamma radiation

The chemical processes have limitations concerning the shape of the nanoparticles, as the shape is very sensitive to changing pH (Patungwasa & Hodak, 2008) and also depends on the reducing agent used (Milligan & Morriss, 1964). In chemical processes for synthesizing stable metallic nanoparticles, it is often necessary to use harsh reaction conditions, such as high temperatures, organic solvents (for example toluene, ethylene glycol or hexadecylamine), very strong reducing agents (for example free electrons in an Mg solution) (Dickerson, Sandhage, & Naik, 2008). The stabilizing agents or reagents used in chemical processes may also end up in the nanoparticle solution, posing a risk to using the nanoparticles in medical applications.

The physical processes have the big disadvantage of needing expensive and very technical equipment. Although physical processes produce very clean solutions without using reducing agents, laboratory equipment is always needed for the synthesis of the nanoparticles. This means that the production of the nanoparticles can never be taken out of a technical laboratory environment (Iravani, Korbekandi, Mirmohammadi, & Zolfaghari, 2014).

The biggest limitation of current nanoparticle production processes is, however, the lack of scalability of the processes. Laboratory techniques only yield 1 g to a maximum of 100 g per batch, resulting in a time-consuming event when in need of a large amount of nanoparticles. The processes are hard to scale up, because the fundamental capability to produce in a large scale, the costs of raw materials, the disposal of waste and environmental issues such as carbon emission are posing problems when the techniques are used at large scale. (Tsuzuki, 2009) Not being able to scale the nanoparticle production processes up results in nanoparticles being expensive and not widely commercially available, which is necessary if nanoparticles were to be used in everyday life.

To further develop the commercial use of nanoparticles, it is critical to develop new methods of production that are reproducible, cheap, environmentally friendly, and safe. As homogeneous nanoparticle size and shape are required for the development of high-performance technologies, new production methods should be reliable and scalable. The technical and commercial restrictions on large-scale production limit the wider use of nanoparticles in the industry.

FORMATION OF NANOPARTICLES IN NATURE: BIOSYNTHESIS

Although one might think that nanoparticles are only producible using laboratory processes, the production of nanoparticles also occurs in nature. Indeed, many different living organisms can produce nanoparticles. Therefore, the biosynthesis of nanoparticles holds promising potential for the development of large scale or commercial production processes.

Biosynthesis of nanoparticles can be found in all sorts of bacteria, yeasts, fungi, plants or algae (Quester, Avalos-Borja, & Castro-Longoria, 2013). Research on nanoparticle biosynthesis has been carried out since the 1980's. For example, Lovley et al. have discovered bacteria that synthesized magnetite nanoparticles intracellularly (Lovley, 1991). Another example is the biosynthesis of gold nanoparticles by the wild-type *E. coli* K12 strain. It was shown that gold nanoparticles can be formed at room temperature using only a pelleted bacterial culture, without the addition of growth media, electron donors or stabilizing agents, and at physiological pH conditions (Srivastava, Yamada, Ogino, & Kondo, 2013). The study of the underlying mechanisms revealed that extracellular membrane-bound proteins were responsible for the biosynthesis of the nanoparticles. This appeared to be true for most cases in which biosynthesis of nanoparticles was shown, opposite to the first assumption that the reduction was caused by enzymatic activity. Thorough research of

the membrane bound proteins revealed that certain peptides are responsible for the synthesis of nanoparticles.

THE BIOSYNTHESIS OF NANOPARTICLES BY PEPTIDES

The peptides responsible for the biosynthesis of the nanoparticles have been closely researched by different groups, but the most insightful research conducted is done by Tan, Lee and Wang. They used a bottom-up approach to identify peptide sequences that can reduce gold ions into nanoparticles.

First, the reduction and binding capability of all natural occurring amino acids was researched. Tryptophan (W) was found to be the fastest reducing agent (figure I6) and was therefore selected as the basis of amino acid mixture studies. The mixture studies were performed to test the influence of the second amino acid on the reduction speed of the mixture (figure I6). It seemed like most of the amino acid mixtures weren't influenced by the presence of another amino acid than tryptophan. These mixtures showed the same reaction time as the pure tryptophan solution. These results suggest that the reaction time of the mixture was determined by the fastest reducing agent.

Reaction Time (hr)	Amino Acid X (0.7 mM of X; 0.1 mM of $HAuCl_4$)	Amino Acid Mixtures (0.4 mM of X ; 0.3 mM of W; 0.1 mM of $HAuCl_4$)
0 ~ 1	W	W, Y, D, F, N, Q, E, P, K, R, G, A, S, V, L, T, I
1 ~ 3	Y	
3 ~ 15	D, F	
15 ~ 24	N, Q, E, P	
24 ~ 30	K, R	
30 ~ 36	G, A	
36 ~ 48	S, V, L	
48 ~ 72	T, I	
72 ~ 336	M, H	M, H
No Reduction	C	C

Figure I6: Different amino acids show different reduction capabilities for the reduction of gold ions into gold nanoparticles. (Tan et al., 2010)

But the effect of the formation of the nanoparticles on the reduction potential of the solution cannot be neglected. As some amino acids (cysteine, histidine and methionine) form strong complexes with metal ions, this would influence the reaction time. Therefore, the effect of a neighboring amino acid, next to tryptophan, was researched next. Peptide sequences XWXWXWX (with X an amino acid other than W) were tested and these showed varying reaction times for different amino acids. This means that reaction kinetics can be influenced by the choice of amino acids to be used in the peptide sequence.

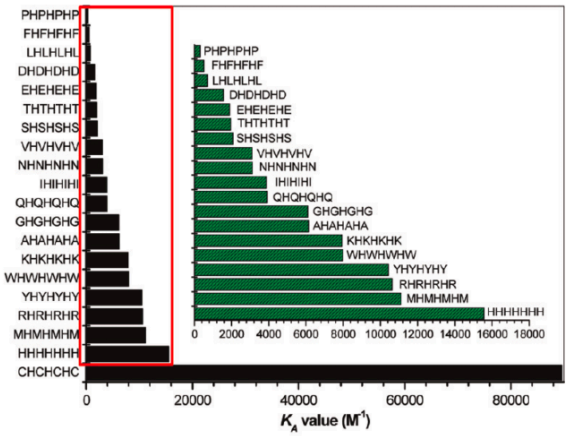

Figure I7: Binding capability of different XHXHXHX peptides. (Tan et al., 2010)

As binding affinity to the gold ions is of importance to the formation of the particles, the binding affinity of all amino acids was tested. As histidine (H) is known to bind to metals strongly, the peptide sequences XHXHXHX (with X an amino acid other than H) were tested for binding affinity to the ions. To do this, the binding constant (K_A) was determined for each variant (figure I7).

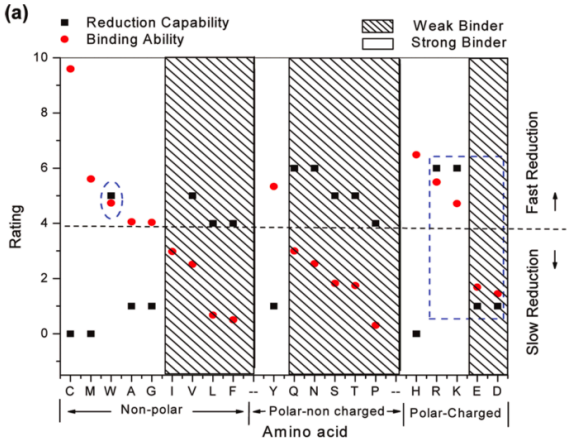

Figure I8: Amino acids organized by reduction and binding capability. (Tan et al., 2010)

Combining the findings on the reduction and binding capability of the amino acids, the consensus was that strong binders have low reduction capability and vice versa. The strong binding, weak binding, fast reducing and slow

reducing amino acids could be named (figure I8). A combination of these amino acids is necessary for successful nanoparticle formation by the peptides. The model proposed by Tan et al. based on this information can be found in figure I9.

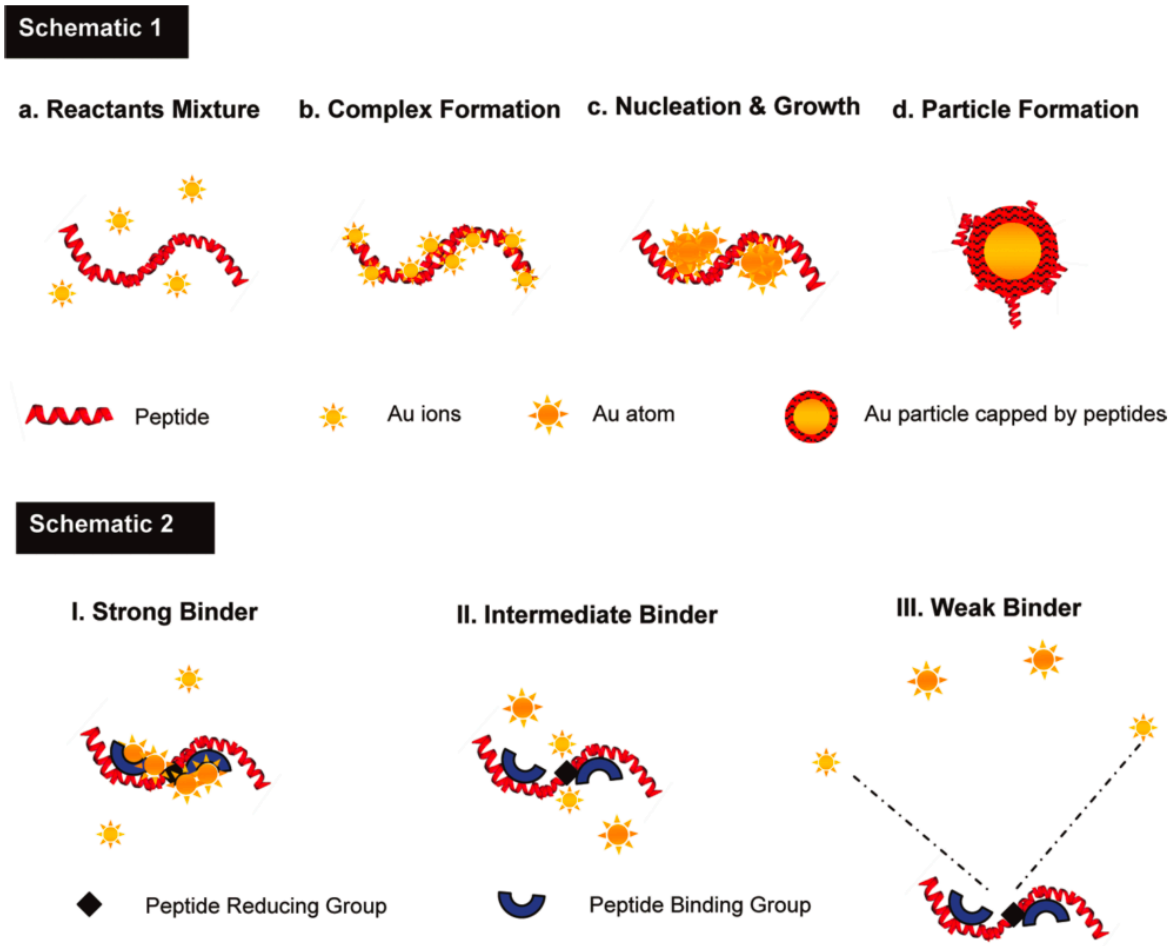

Figure I9: schematic 1 shows the proposed model of nanoparticle formation by reducing peptides in aqueous solution. The $AuCl_4^-$ ions are bound to the peptide (b), if the binding of the complex to the ions is too strong, reduction won't be possible. Schematic 2 shows the mechanism that determines the binding capability of the peptide. If the binder is too strong, the ions will not be able to reach the reducing group of the peptide. If the binder is too weak, the ions are not attracted to the peptide enough for reduction. (Tan, Lee, & Wang, 2010)

ADVANTAGES AND LIMITATIONS OF BIOSYNTHESIS OF NANOPARTICLES

Advantages of biosynthesis of metallic nanoparticles include that it is cheaper than physical or chemical production, as bacteria can be grown cheaply without too many resources. Furthermore, there is no need for extreme pH values or temperatures when using biosynthesis. And when using reducing peptides, the reducing agent becomes unnecessary. However, the yield of biosynthesized nanoparticles is still low, the process is slow (several hours to days) and control over the shape and size of the resulting particles is poor when compared to chemical or physical production processes (Li, Xu, Chen, & Chen, 2011).

Biosynthesis could be a very important commercial nanoparticle production process if the limitations, low yield, a long reaction time and poor shape and size control, are overcome.

PROTEIN CAGES AS NANOREACTORS FOR NANOPARTICLE FORMATION

VIRAL CAPSIDS AS PROTEIN CAGES

As shape and size uniformity are very important for nanoparticle solutions, the ability to control shape and size by restricting the nucleation to a maximum size would be very convenient. This restriction can be implemented by using protein cages in which a nanoparticle can be synthesized.

In nature, protein cages are often found in the form of viral capsids, the protein capsule that surrounds and protects the viral DNA or RNA. Empty viral capsids make ideal protein scaffolds for synthesizing nanoparticles, as they are found in many sizes in nature and have a structure that allows access to the capsid interior (Douglas et al., 2002). For example, Douglas et al. used the cowpea chlorotic mottle virus capsid, a capsid counting 180 identical 20 kDa subunits that self-assemble into a 28 nm large structure. They set out the goal to mimic the activity of the iron storage and mineralization protein ferritin, especially the L-chain of ferritin. The L-chain of ferritin forms nanoparticles of iron oxide within its shell. They showed that their engineered capsid restrained both the size and the shape of the formed nanoparticle.

Another big advantage of using capsids as nanoreactors, is that capsids are easy and cheap to produce using simple expression protocols in bacteria.

NANOPARTICLE PRODUCTION IN CAPSIDS USING REDUCING PEPTIDES

It has been shown on one hand that size-constricted nanoparticle production in viral capsids is possible using an added reducing agent. On the other hand, we know that peptides are able to reduce metal ions to metallic nanoparticles. We want to combine the capsids with the reducing peptides to make a simple nanoreactor, which forms nanoparticles upon addition of metal ions without using a chemical reducing agent. With this approach, we can combine the advantages of the use of viral capsids (cheap, easy to produce and available from nature in many different sizes) with those of the reduction of metal ions using peptides (no use of a reducing agent). The novel part of this approach is the display of the reducing peptides at the inner surface of the capsids and the combination will enable nanoparticle formation that is restricted in size and shape. Our capsids will be able to produce the nanoparticle by reduction of metal salts, stabilize the nanoparticle and with minor genetic modification, can be decorated on the exterior of the capsid.

Decoration of the outside of the capsid is common (Schwarz et al., 2015), a target protein is fused to the outside of the capsid via a decoration protein. This target protein can target different proteins of interest, for example in targeted drug delivery.

IMPLEMENTATION

We propose to implement this proof of principle project by designing and expressing engineered protein cages in *E. coli*. *E. coli* is chosen as chassis, because the bacteria are easy and fast to grow, widely available and a lot is known about the genetic engineering of this bacterium. *E. coli* are often used for protein expressions because of these properties and is the best suited chassis for our proof-of-concept project.

The protein cages we propose to use are empty virus capsid, built up out of monomers that self-assemble into a capsid. To express our peptides on the inside of the capsids, the monomers need to be modified. We will do this by genetically engineering the monomer proteins and fusing our metal reducing peptides to the monomer.

The expression and self-assembly of the protein capsids will take place within the bacterium while the synthesis of the nanoparticle itself happens in a purified capsid solution with a metal salt solution added. This is done because of the toxicity of the metal ions for the bacterial cells (Zhao & Stevens, 1998).

SCOPE OF THE THESIS

In this thesis, the goal is to produce silver and gold nanoparticles using peptides fused to the inside of protein cages, that therefore act as scaffolds. We want to demonstrate the size-constrained synthesis of metallic nanoparticles inside our engineered capsids. To prove this concept, silver and gold nanoparticles have been selected and two different capsids will be selected. Silver and gold nanoparticles were selected with multiple reasons; silver and gold nanoparticles are among the most studied metallic nanoparticles, as they have potential for use in medical treatments. Silver nanoparticles even have antimicrobial applications, as leaking silver ions have toxic effects on bacteria (Zhao & Stevens, 1998).

To achieve this goal, several steps need to be taken. First, the appropriate peptides need to be found for the reduction of the silver and gold ions into nanoparticles. Next, the appropriate protein cages need to be selected and the peptides need to be fused to the protein cages. To make sure the protein cage can act as a scaffold for the production of nanoparticles, we need to check if the modified protein cages still self-assemble. If self-assembly is verified for the modified cages, the next step is to verify nanoparticle formation by the protein cages.

MATERIALS AND METHODS

MATERIALS

STRAINS

Escherichia coli DH5α was used for cloning purposes. *E. coli* BL21 was used for carrying out the experiments. All strains were always grown on LB medium, when needed with 50 μg/ml kanamycin added.

PLASMIDS

All used plasmids are listed in table M1. All plasmids have a kanamycin resistance and a ColE1 origin of replication. Plasmid maps can be found in Appendix 1. Primers used for the project can be found in Appendix 2.

Table M1: Plasmids used for the project.

Plasmid	Description
pMS2-WT	MS2 WT (capsid protein) controlled by lacUV5 promoter
pMS2-AG4	MS2 with AG4 inserted controlled by lacUV5 promoter
pMS2-AGP35	MS2 with AGP35 inserted controlled by lacUV5 promoter
pMS2-AUSE	MS2 with AUSE inserted controlled by lacUV5 promoter
pMS2-AURW	MS2 with AURW inserted controlled by lacUV5 promoter
pP22-WT	P22 CP SP_{141} (capsid protein and truncated scaffold protein) controlled by lacUV5 promoter
pP22-AG4	P22 CP SP_{141}-AG4 controlled by lacUV5 promoter
pP22-AGP35	P22 CP SP_{141}-AGP35 controlled by lacUV5 promoter
pP22-AUSE	P22 CP SP_{141}-AUSE controlled by lacUV5 promoter
pP22-AURW	P22 CP SP_{141}-AURW controlled by lacUV5 promoter
pETMS2-WT	MS2 WT (capsid protein) controlled by T7 promoter
pETMS2-AG4	MS2 with AG4 inserted controlled by T7 promoter
pETMS2-AGP35	MS2 with AGP35 inserted controlled by T7 promoter
pETMS2-AUSE	MS2 with AUSE inserted controlled by T7 promoter
pETMS2-AURW	MS2 with AURW inserted controlled by T7 promoter

SOLUTIONS

LB MEDIUM

For all cell cultures Lysogeny Broth medium was used. LB medium is made with 10 g/L tryptone, 5 g/L yeast extract and 10 g/L NaCl, solved in MilliQ water.

TSS BUFFER

100 mL of TSS buffer is made with 10 g PEG 3350, 5 mL DMSO, 2mL 1M $MgCl_2$ and LB medium until 100 mL. It is filter sterilized and stored at 4°C.

5X KCM BUFFER

The transformation protocol makes use of 5X KCM buffer. This buffer is made of 500 mM KCl, 150 mM $CaCl_2$ and 250 mM $MgCl_2$.

LYSIS BUFFER

Lysis buffer is made by adding 50 mM HEPES buffer (Sigma-Aldrich), 100 mM NaCl and 2 mM EDTA to MilliQ water. Afterwards it is filter sterilized using the vacuum pump.

METHODS

CLONING PROTOCOLS

PRIMERS

Primers were ordered at Integrated DNA Technologies and upon reception, made into a 100 µM primer stock using MilliQ water. All processes following use a 10 µM primer stock, made by diluting the 100 µM primer stock 10 times with MilliQ water.

PHUSION PCR

For PCRs with template DNA, the Thermo-Fisher Scientific PCR Phusion kit was used with a primer concentration of 0.5 µM and 50 ng of template DNA. DMSO was added in case of the use of GC-rich primers. Both an Applied Biosystems Veriti 96 well Thermal Cycler and a Biorad C1000 Touch Thermal Cycler were used. The cycle used: 98°C 30s; 98°C 10s, Tann 30s, 72°C 30s per kb (35x); 72°C 7 min; 4°C indef. When applicable, DpnI digestion was used. In that case, 1 µL of DpnI (Thermo-Fisher Scientific) was used and incubated for a minimum of 2 hours at 37°C.

AGAROSE GEL

Agarose gels were used to separate the DNA fragments from Phusion PCR or colony PCR. A 1% agarose gel is made by adding 0.5 g agarose (Sigma-Aldrich) to 50 mL TAE buffer (Promega, 40x TAE buffer molecular biology grade), solving the agarose using the microwave, cooling down until about 50°C and adding SYBRsafe (Thermo-Fisher Scientific). In case of Phusion PCR, the product is mixed with Promega blue/orange 6x loading dye and run in an Thermo Scientific Owl Easycast B1A gel container at 115V and 500mA for 20 or 30 minutes (depending on if one or two rows of wells were used). In case of colony PCR, no loading dye is added. In both cases, the Fisher Scientific EXACTgene 1kb plus ladder is used.

GEL PURIFICATION

Gel purification was done using the Wizard Promega Gel and PCR clean-up system. The standard protocol supplied by the company was used, with a few adjustments: use 500 µL of membrane binding solution and for elution of the DNA use 25 µL of warm water and a 10 minute incubation step.

DNA CONCENTRATION MEASUREMENT

The concentration of purified DNA was measured using the Thermo Scientific Nanodrop 2000 Spectrophotometer.

SLICE

A SliCE reaction (Zhang, Werling, & Edelmann, 2012) was performed on DNA fragments to construct the plasmids (figure M1). SliCE is a quite recently discovered cloning method, in which overlaps are created using primers with a tail containing 15 basepairs or more of homology. SLiCE can be used to assemble multiple inserts into a backbone at once, without the need for multiple reactions. Assembly is done by a simple incubation step. For the reaction, add together: 50 to 200 ng of vector backbone, 1:5-1:10 ratio of insert(s) (calculated by the formula $\frac{length\ insert\ (kb)}{length\ vector\ (kb} * ng\ of\ vector\ DNA = ng\ of\ insert\ DNA\ for\ a\ 1{:}1\ ratio$), SliCE buffer and PPY SliCE extract, the mixture is incubated at 37°C for 1 hour.

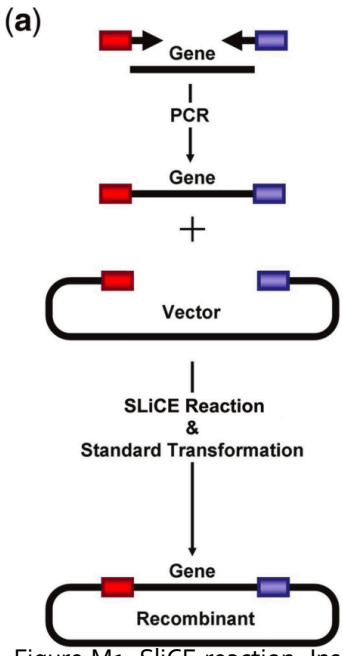

Figure M1: SliCE reaction. Inserts and vector are amplified using Phusion PCR. When combined, the DNA binds using homology. (Zhang et al., 2012)

TRANSFORMATION

Transformation in competent *E. coli* DH5α or BL21 cells. This is done by adding the DNA after SliCE (10 µL), 20 µL 5x KCM buffer and 70 µL MilliQ water to 100 µL DH5α cells and incubating on ice for 30 minutes. The BL21 cells are used after the DNA has been confirmed by sequencing. In this case 1 µL of plasmid DNA is added to 20 µL 5x KCM buffer, 79 µL MilliQ water and 100 µL BL21 cells. The same incubation step is used. After this, the cells undergo heat shock for 90 seconds at 42°C and 1 hour incubation at 37°C in 400 µL LB medium. Afterwards the cells are plated on selective medium plates and grown overnight at 37°C.

COLONY PCR

The transformed DH5α colonies were tested for the insert using colony PCR and appropriate primers. Colony PCR involves using Thermo-Fisher Scientific DreamTaq Green MasterMix with a cycle of 95°C 8 min; 95°C 30s, Tann 30s, 72°C 1 min/kb (35x); 72°C 5 min; 4°C indef. The colony PCR was run on a 1% agarose gel as described before and an image was made of the result.

ISOLATION OF PLASMID DNA

Colonies containing the insert (as confirmed by colony PCR) are grown overnight in LB, isolated using the Promega Wizard Plus SV Minipreps and sent for sequencing with appropriate primers. The standard protocol supplied by the company was used, with a few adjustments: 4 mL of overnight culture was used and upon elution 30 µL of warm water was added and the column was incubated for 10 min at room temperature.

SEQUENCING OF PLASMID DNA

DNA was sent for sequencing using the Macrogen EZ-seq sequencing service. DNA was supplied with a primer as specified by Macrogen.

COMPETENT CELL PRODUCTION

The empty strain is inoculated in 5 mL LB from a single colony and grown overnight. LB medium in a baffled flask is inoculated 1:100 with overnight culture and grown at 37°C and 250 rpm until OD_{600} is between 0.3 and 0.4. The culture is chilled on ice for a minimum of 20 minutes and centrifuged at 8000g and 4°C for 8 minutes. The supernatant is thrown away and the pellet is resuspended in $1/10^{th}$ volume of the used culture of ice-cold TSS buffer. 100 µL aliquots are made, flash frozen in liquid nitrogen and stored at -80°C.

CAPSID EXPRESSION PROTOCOL

The BL21 cells with the correct plasmids inserted were grown overnight in LB, inoculated 1:100 to make a large culture (200 mL or 500 mL) and grown at 37°C 200 rpm until OD_{600} ~0.5. After inducing with IPTG (0.25 mM final concentration), the cultures were grown at 30°C 200 rpm for 18 hours. Cultures were then harvested via centrifugation for 30 min at 4000 rpm and 4°C. Pellets were frozen at -20°C or directly used for capsid purification.

CAPSID PURIFICATION PROTOCOL

CAPSID EXTRACTION

Extraction of the capsids starts with thawing the pellets on ice, resuspending in 4 mL lysis buffer for each 50mL of culture used to get the pellet. Lysozyme (chicken lysozyme, Sigma-Aldrich) was added (1 mg/mL final concentration) and incubated on ice for 30 min. Afterwards the samples were sonicated (PTS technics Qsonica sonicators), using one of the following settings:

- Method 1: sonication in 4mL "portions" – sonication for 2 min pulse time in pulses of 30 seconds (15 seconds off) and power amplitude 50%.

- Method 2: sonication in 16 mL "portion" – sonication for 6 min pulse time in pulses of 30 seconds (15 seconds off) and power amplitude 50%.

After sonication DNaseI and RNase (final concentration 10 µg/mL) were added, followed by incubation on ice for 20 min. Cell debris was removed via centrifugation at 14000 rpm and 4°C for 40 min to 60 min. The supernatant was used for capsid precipitation using 0.1 g NaCl and 0.5 g PEG-8000 (Sigma-Aldrich) per 4 mL of supernatant and this was incubated overnight at 4°C while gently shaking. The precipitate was collected by centrifugation for 40 min at 14000 rpm 4°C and resuspended in 1.5 mL HEPES buffer per 16 mL of lysate used (originating from 200 mL of culture) and filtered using a protein LoBind filter of 0.2 µm.

SIZE-EXCLUSION CHROMATOGRAPHY

To further purify the capsid solutions, the AKTA (GE Healthcare ÄKTA pure) can be used. AKTA is a size-exclusion chromatograph, in which proteins are flushed trough a column. The retention time depends on the size of the proteins, with smaller proteins taking longer than larger proteins. The protocol developed for the AKTA machine was based on literature (Tobias W. Giessen & Silver, 2016) and on the manual of the HiPrep column (GE Healthcare HiPrep 16/60 Sephacryl S-300 High Resolution) we used. A flow rate of 0.8 mL/min and HEPES buffer were used. In total 1.4 column volume (one column volume is 120 mL) of buffer was run through the column with a starting sample of 1 mL capsids. Fractions of 2 mL were collected.

PROTEIN CONCENTRATION

The protein concentration was measured using the Bio-Rad Bradford kit and protocol. Samples are prepared according to the pipetting scheme in table M2. The protein standard used is bovine gamma-globulin.

Table M2: Bradford assay pipetting scheme.

Name	Concentration [µL/mL]	Water [µL]	Protein standard/sample [µL]	Reagent [µL]
C0	0	800	0	200
C1	1.4	799	1	200
C2	2.8	798	2	200
C3	4.2	797	3	200
C4	8.4	794	6	200
C5	21	785	15	200
QC1	3.5	797.5	2.5	200
QC2	7	795	5	200
Sample	calculate	799	1	200

After adding all the components, the samples are vortexed and left to incubate for 10 minutes. The samples are transferred to cuvettes and the A_{595} is measured using the Nanodrop. After verification of the R^2 and the QC absorbance, the protein concentration can be calculated by multiplying by 1000. This is the protein concentration in mg/mL.

CHARACTERIZATION PROTOCOLS

SDS-PAGE GEL

To confirm capsid production, the purified capsids both before and after AKTA were run on SDS-PAGE protein gels (Bio-Rad mini-protean TGX stain-free gels 4-20%) at 200 V for 15 min to 20 min with a Bio-Rad precision plus protein unstained standards ladder in 1x TGS buffer (50x molecular biology grade Promega). The samples were diluted 1:1 with loading buffer, containing 5 µL 4x Laemmli buffer (Bio-Rad), 4 µL 250 mM DTT and 1 µL MilliQ water.

METAL SALT ASSAY FOR SILVER NANOPARTICLES

Capsids obtained with the capsid production protocol were added to different concentrations of $AgNO_3$ salts in HEPES buffer. The samples were prepared in a Greiner 96-well black plate with transparent bottom and incubated in the dark at 37°C for 24 hours.

CELL EXTRACT ASSAY FOR SILVER NANOPARTICLES

A cell extract of *E. coli* cells was used to screen for the production of silver nanoparticles. The extract was "Pepe" extract obtained from David Foschepoth (TU Delft, BN department, Christoph Danelon lab). The following was added together: HEPES buffer 50 mM, K-glutamate 90 mM, Mg-glutamate 15 mM, Aminoacids 1 mM, 5x basis 1 mM, lysate 1 mM and DNA 2 ng/µL. With MilliQ water the volume was brought up to 100 µL per well. The mix was incubated for 6 hours at 30°C, then silver salts ($AgNO_3$) were added in a concentration of 100 mM and the reaction was left for 24 hours in the dark at 37°C. To read the results, the samples were prepared in a Greiner 96-well black plate with transparent bottom and read using the Tecan platereader.

UV-VIS SPECTROSCOPY

UV-VIS spectroscopy was completed with a Tecan platereader, measuring the absorbance spectrum from 230 nm to 700 nm with stepwise increases of 10 nm.

RESULTS

SELECTION OF THE CHASSIS AND PHAGES

The self-assembling capsids for the project were chosen from literature, being the MS2 *E. coli* RNA phage and the *Salmonella* p22 dsDNA phage.

MS2

The MS2 *E. coli* RNA phage has a capsid that consists of 180 identical capsid protein monomers of 13 kDa, which self-assemble into an isocahedral capsid with an outer size of 27 nm and inner size of 21 nm. Each monomer of MS2 has two loops that can be modified, one on the exterior of the capsid and one in the interior. It has been shown that insertions in the inner loop allow encapsulation of cargo proteins within the capsid (figure R1) (Tobias W. Giessen & Silver, 2016). The MS2 capsids still self-assembly with the modification of the capsid protein monomer.

Our reducing peptides can be added within the interior insertion loop directly and will be expressed on the inside of the self-assembled capsids.

The interior insertion loop is defined between the serine at site 52 and the glutamine at site 55 of the MS2 capsid protein.

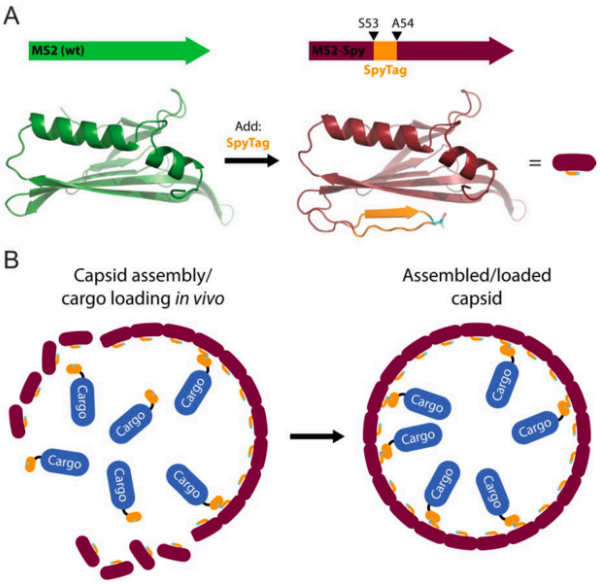

Figure R1: Encapsulation of a cargo protein inside MS2 by insertion of a short protein in the interior insertion loop of the MS2 monomer. (Tobias W. Giessen & Silver, 2016)

P22

The *Salmonella* p22 phage has a capsid that consists of 420 capsid proteins (47 kDa) and around 300 scaffolding proteins. Together these self-assemble into a capsid with an outer size of 64 nm and an inner size of 54 nm. It has been shown that the scaffolding proteins can be truncated without influencing the self-assembly of the capsid (Parker, Casjens, & Prevelige, 1998). The scaffolding protein is truncated by removing amino acids 1 to 140 and leaving the amino acids 141 to 303 intact (resulting in a molecular weight of 18 kDa). The peptides were fused directly to the scaffolding proteins by inserting the gene coding for our peptide and a simple GS linker between the codons for amino acids 141 and 142.

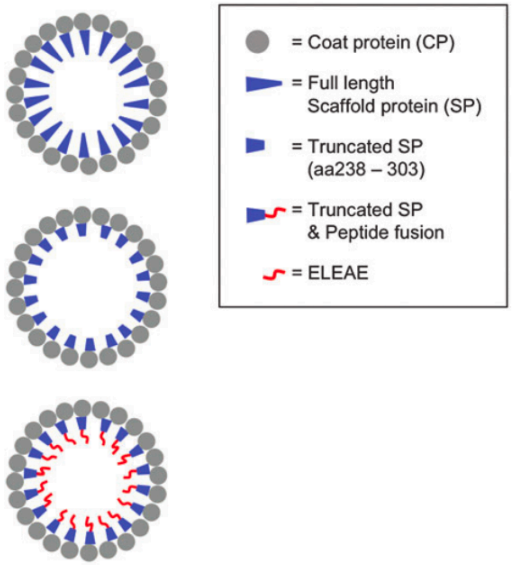

Figure R2: Fusion of a peptide to the truncated protein of the P22 capsid. In our case the truncated protein had amino acids 141-303. (Reichhardt et al., 2011)

SELECTION OF THE REDUCING PEPTIDES

Two of the most used metal nanoparticles are golden and silver nanoparticles. They are widely used in research and are still expensive to produce at this moment. For the formation of the nanoparticles, reducing peptides were selected that reduce metal ions to metal.

SILVER REDUCING PEPTIDES

The silver reducing peptides AG-4 and AG-P35 were selected because of their proven ability to synthesize metallic silver particles from silver ions in aqueous solution (R. R. Naik et al., 2004). The peptide solutions (10 mg/mL) were incubated with 0.2 mM silver nitrate in 0.1M HEPES buffer (pH 7.5) for 24 to 48 hours at room temperature. After 24 hours the solutions changed color and the samples were analyzed. To confirm that the silver nanoparticles were produced, a combination of UV-vis spectrometry and TEM was used.

The AG4 solution showed a peak at 420 nm absorbance for the UV-vis spectrometry (figure R3a) and the TEM images (figure R3b) showed multiple shapes of nanoparticles, such as spheres, triangles and hexagons with an average size of 102±28 nm (Rajesh R. Naik, Stringer, Agarwal, Jones, & Stone, 2002).

The AG-P35 solution showed a peak at 430 nm for the UV-vis absorbance spectrometry. The TEM images showed spherical shapes and it was confirmed with another assay that the particles seen contained silver. The size of the particles produced is 52±13.2 nm, about half of the size of the AG4 particles (R. R. Naik et al., 2004).

The amino acid sequences of the AG4 and AG-P35 peptides are:

AG4	*NPSSLFRYLPSD*
AG-P35	*WSWRSPTPHVVT*

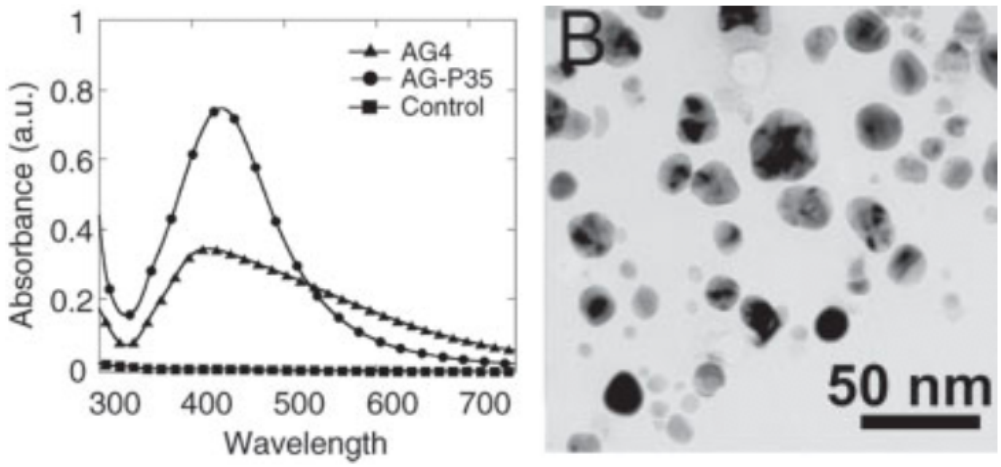

Figure R3: a) UV-VIS spectrum of the nanoparticles produced with AG4 and AG-P35 peptides in aqueous solution. b) TEM image of the nanoparticles produced by AGP-35 peptides. (R. R. Naik et al., 2004)

GOLD REDUCING PEPTIDES

The gold reducing peptides were selected from (Tan et al., 2010), in which a bottom-up approach was used to design peptides that were able to reduce gold ions into metallic gold. Not only were the peptides designed, but also characterized by reaction time and size of the resulting nanoparticles. The reactions were carried out in aqueous solutions with 0.1 mM $HAuCl_4$ and 0.1 mM peptide (AURW) or 0.3 mM peptide (AUSE), pure water was the only solvent used. The reaction time and result strongly depend on the reduction and binding capabilities of the amino acid tested, the consensus found was that strong binding amino acids have a low reduction capability and that weak binding amino acids have a high reduction capability.

It was found that tryptophan (W) has a high reduction capability, while still binding quite strongly. The peptide *RWRWRWR* was named as favorable for the reduction reaction, because it is a positively charged peptide, which can attract the gold ions used ($AuCl_4^-$), as they are negatively charged. Based on an earlier study of (Brown, Sarikaya, & Johnson, 2000), the two sequences *SEKL* and *GASL* were used to research the variations in reaction time of production and size of the gold nanoparticles. Using *SEKL* and *GASL* repeats, Brown et al. produced quite large nanostructures, which could be explained by the fact that the repeats contained many strong binders, slowing the reaction time down. By adding two tryptophan in between the *SEKL* and *GASL*, the reaction was sped up to about 4 hours, resulting in nanoparticles with an average size of 40 nm. This size corresponded roughly with the desired size of the particles inside the capsids and therefore the peptide *SEKLWWGASL* was used as well.

"AUSE"	*SEKLWWGASL*
"AURW"	*RWRWRWR*

The UV-VIS spectra and the self-assembly confirmed by TEM can be found in figures R4 and R5 for both peptide sequences.

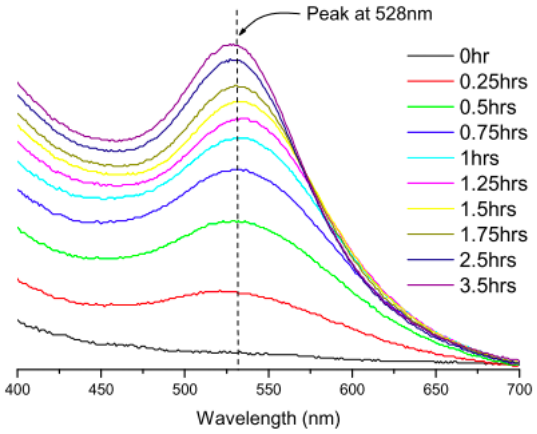

Figure R4: UV-vis spectrum of the nanoparticles produced by the peptide RWRWRWR (AURW). (Tan et al., 2010)

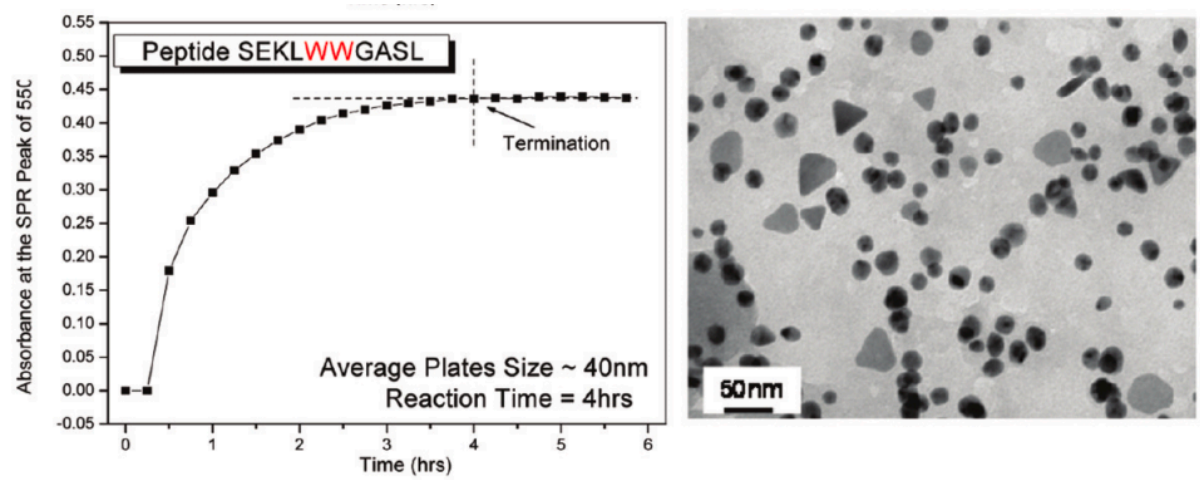

Figure R5: a) Absorbance of the nanoparticles produced by the peptide AUSE at 539 nm. b) TEM of the nanoparticles produced by the peptide AUSE. (Tan et al., 2010)

FUSING THE PEPTIDES TO THE CAPSID MONOMERS

MODELLING THE PROTEIN STRUCTURE OF MS2 MONOMERS

As self-assembly of the MS2 monomers is vital for the proof of our concept, the structure of the MS2 monomers need to be as close to the WT as possible. This will ensure correct self-assembly of the capsid. If the monomers have secondary or tertiary structures that differ too much from the WT monomer, self-assembly of the capsid could be disrupted.

As there are three possible insertion sites in the inner insertion loop of the MS2 monomer (S52S53, S53A54 and A54Q55) (figure R6), the proteins need to be modeled to make sure only viable options are tested in the lab. Depending on the models that are obtained, it is decided which variants are cloned in the lab.

There are some easy tools that enable fast visualization of protein models. The amino acid sequence of the desired monomers was fed to the online protein modeler Phyre2 (Kelley, Mezulis, Yates, Wass, & Sternberg, 2015). Phyre2 then provided 3D protein models based on the entered amino acid sequence. This could then be visualized with Chimera software (Pettersen et al., 2004).

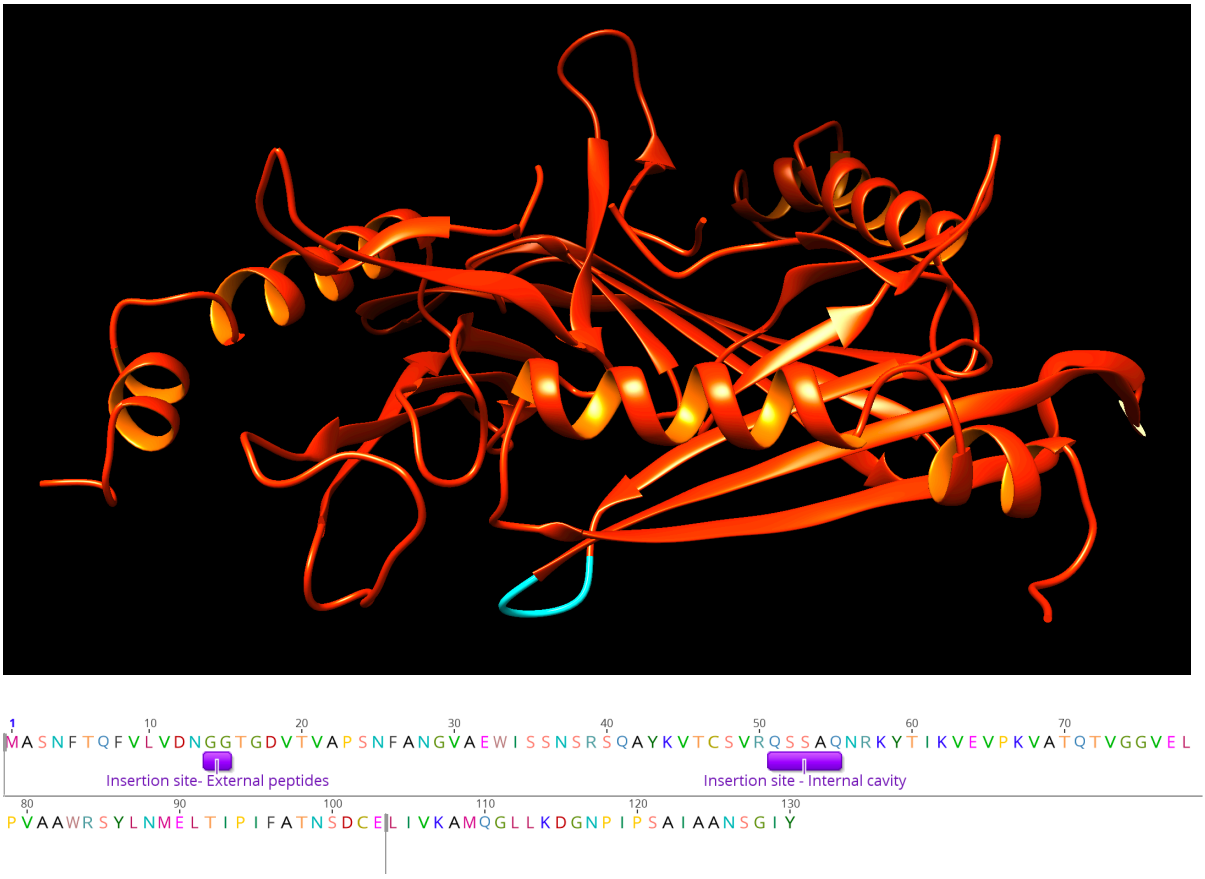

Figure R6: a) protein model of three MS2 WT monomers. The interior insertion loop is shown in cyan. b) amino acid sequence of MS2 WT. The insertion sites are annotated in purple.

MONOMERS WITH THE SILVER REDUCING PEPTIDES

From the protein models of the different variants, the most promising model of each variant was chosen to work with. The choice was based on the difference in three-dimensional structure between the variant and the wildtype. For AG4 (figure R7) the insertion site between S53 and A54 seemed the best option. Because the S52S53 model shows our AG4 peptide folding inwards towards the bulk of the protein, threatening the activity of the peptide and self-assembly of the monomers. The A54Q55 shows an unwanted helical structure in the inserted loop, which can drastically change our peptides activity.

AGP35 (figure R8) shows some big alterations in the helical structure preceding the insertion site for the S52S53 and S53A54 insertions. The A54Q55 doesn't show this alteration in helical structure and doesn't show any added other secondary structures, therefore A54Q55 was chosen for the insertion of AGP35.

Figure R7: protein models of MS2-AG4 (blue) and MS2-WT (red) at different insertion sites. Confidence level: 91% of the structure modelled with >90% confidence.

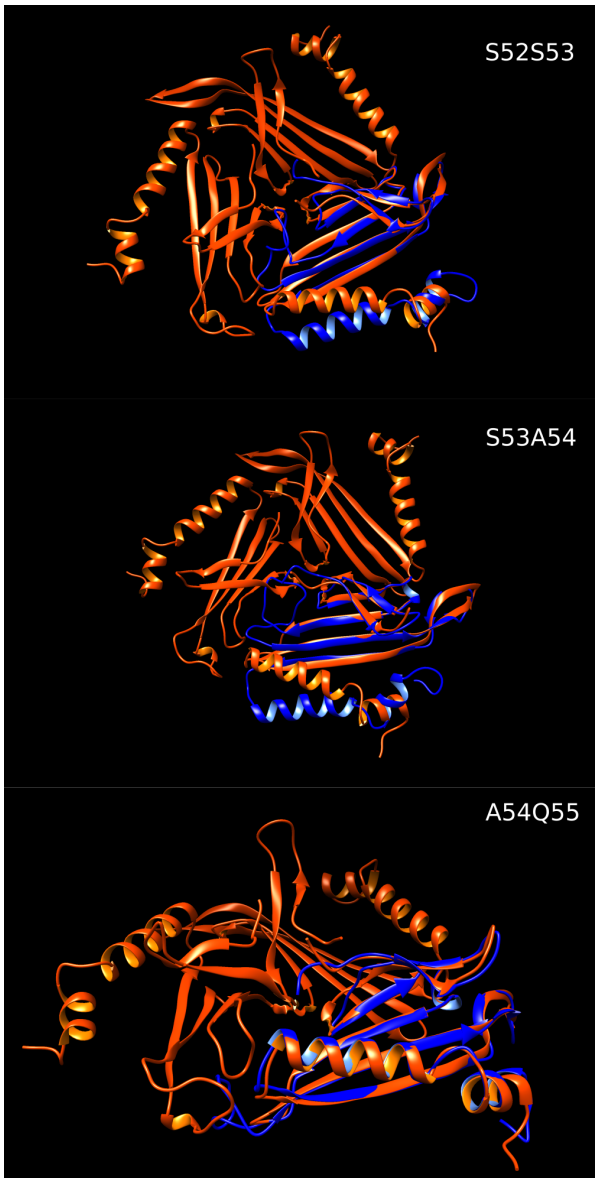

Figure R8: protein models of MS2-AGP35 (blue) and MS2-WT (red) at different insertion sites. Confidence level: 91% of the structure modelled with >90% confidence.

MONOMERS WITH THE GOLD REDUCING PEPTIDES

The AUSE (figure R9) insertion A54Q55 was chosen as the best option, because the tertiary structure of the protein is the most similar to the wildtype MS2 monomer. When the insertion is placed at S52S53, the reducing peptide (loop) turns inwards, posing a risk to the activity of the peptide. At insertion site S53A54, an unwanted secondary helical structure arises and the secondary structure in other parts of the protein is severely influenced.

AURW (figure R10) is the smallest peptide inserted of all four, which results in less distortion of the protein tertiary structure. Eventually insertion site S53A54 was chosen as best option, because the loop with the peptide protrudes to the interior of the capsid the most. Also S52S53 shows an elongated plate secondary structure just after the insertion site, making it a less suitable option.

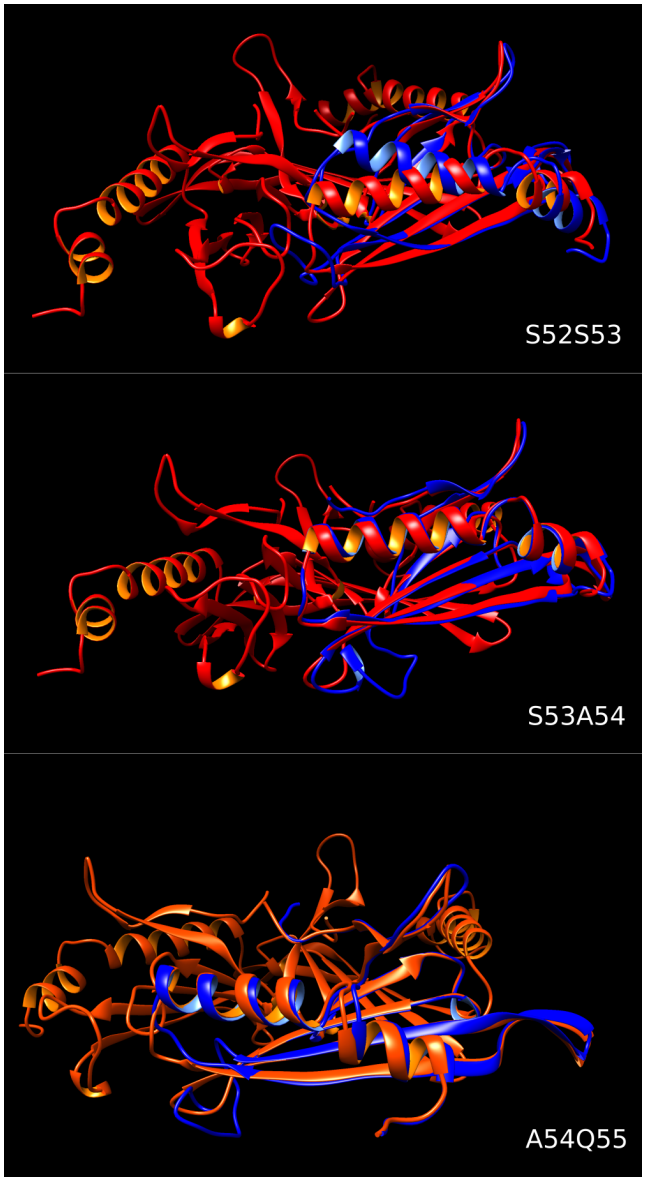

Figure R9: protein models of MS2-AUSE (blue) and MS2-WT (red) at different insertion sites. Confidence level: 92% of the structure modelled with >90% confidence.

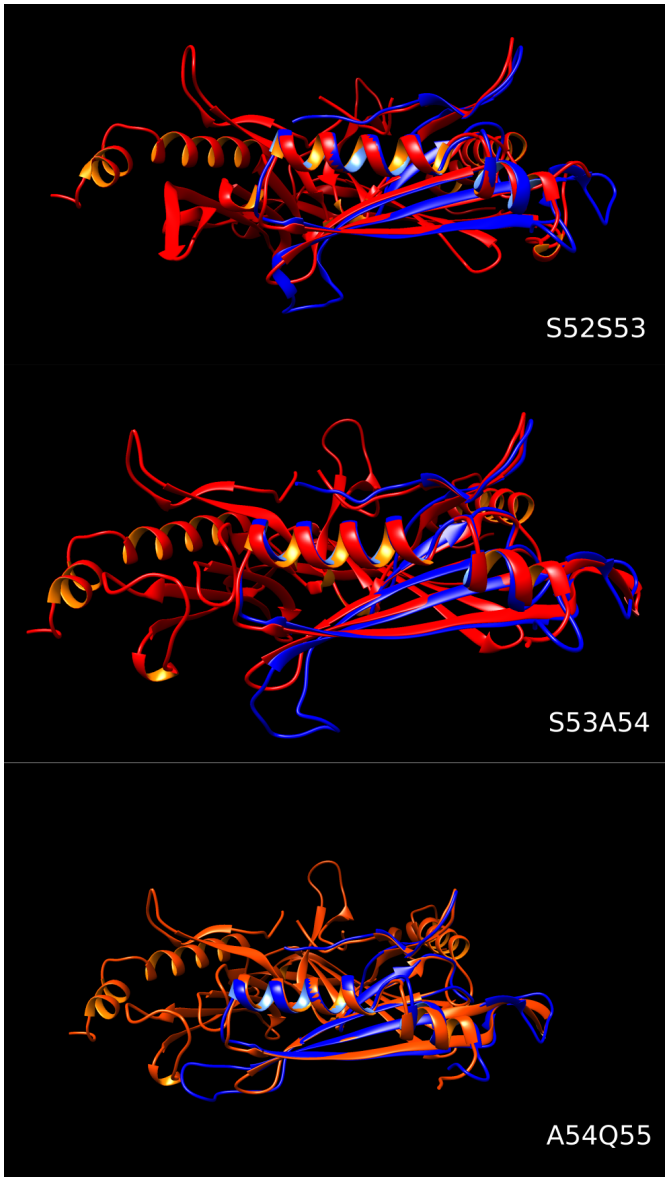

Figure R10: protein models of MS2-AURW (blue) and MS2-WT (red) at different insertion sites. Confidence level: 95% of the structure modelled with >90% confidence.

FUSING THE PEPTIDES TO THE TRUNCATED SCAFFOLD PROTEIN OF P22

For P22 the procedure was much simpler, the peptides were added to the amino acid sequences between site 141 and 142. A GS linker was added between the scaffold protein and the reducing peptide. For P22 there is no need to model the proteins, as the secondary and tertiary structures of the SP_{141} are not influenced by the addition of the peptide.

MOLECULAR CLONING OF MODIFIED MONOMERS

We aim to insert the coding sequence of the peptide to the MS2 capsid protein gene and the P22 truncated scaffold protein gene.

First, we codon optimized each of the peptides for expression in *E. coli.* The tool of Integrated DNA Technologies (extra reference 4). After this we also codon optimized the P22 and MS2 proteins for expression in *E. coli*. The WT capsid genes were cloned in high copy number vectors (colE1) under the IPTG inducible lacUV5 promoter, carrying a kanamycin resistance cassette. The resulting plasmids are pMS2 and pP22 (figure R11). All plasmids were designed using Geneious software (extra reference 5).

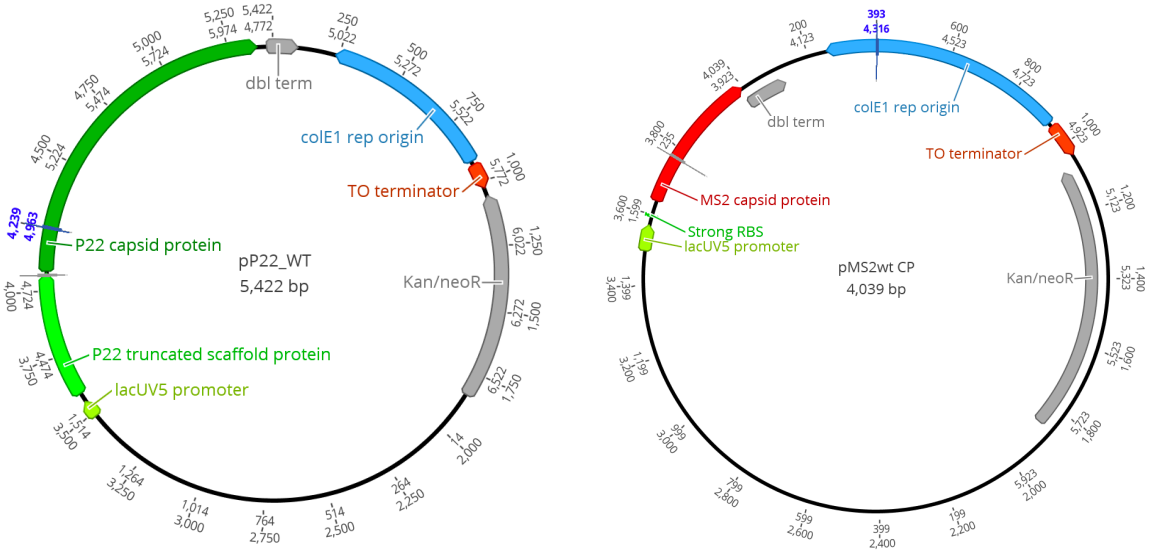

Figure R11: Plasmid designs of the P22 and MS2 WT plasmids.

The fusions of the peptides and the P22 and MS2 proteins were cloned using SliCE. The resulting constructs were (for plasmid maps consult appendix 1):

- MS2
  - pMS2-AG4
  - pMS2-AGP35
  - pMS2-AUSE
  - pMS2-AURW
- P22
  - pP22-AG4
  - pP22-AGP35
  - pP22-AUSE
  - pP22-AURW

VERIFYING EXPRESSION OF THE CAPSIDS

To test expression of the MS2 WT and P22 WT, AG4, AGP35 and AUSE capsids, cultures of BL21 cells with these plasmids were made. The cultures were induced with IPTG and after incubation the cells were isolated by centrifugation. The pellets were used for the extraction of the capsids using the capsid extraction protocol. The expression of the proteins was visualized using an SDS-PAGE gel (figures R12 and R13) and the P22 WT capsid sample was visualized using TEM (figure R14).

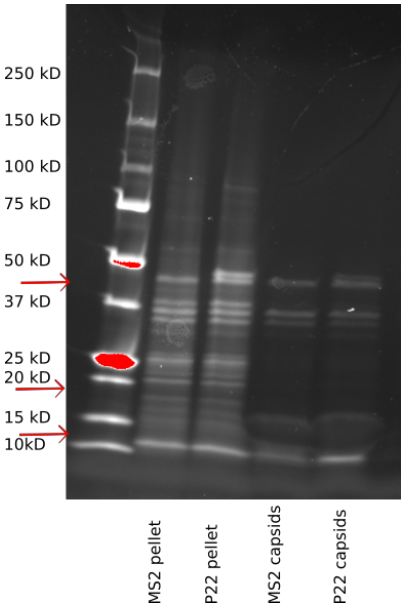

Figure R12: SDS-PAGE of MS2 and P22 pellets and capsid solutions. The "pellet" samples were scrapings directly taken from the pelleted bacterial cultures and then boiled for 10 minutes at 95°C. The "capsids" samples were directly loaded from the extracted capsid solutions. MS2 monomers have a molecular weight of 13 kDa, P22 capsid protein subunits weigh 47 kDa and the SP_{141} weighs 18 kDa for the WT. Red arrows indicate expected bands.

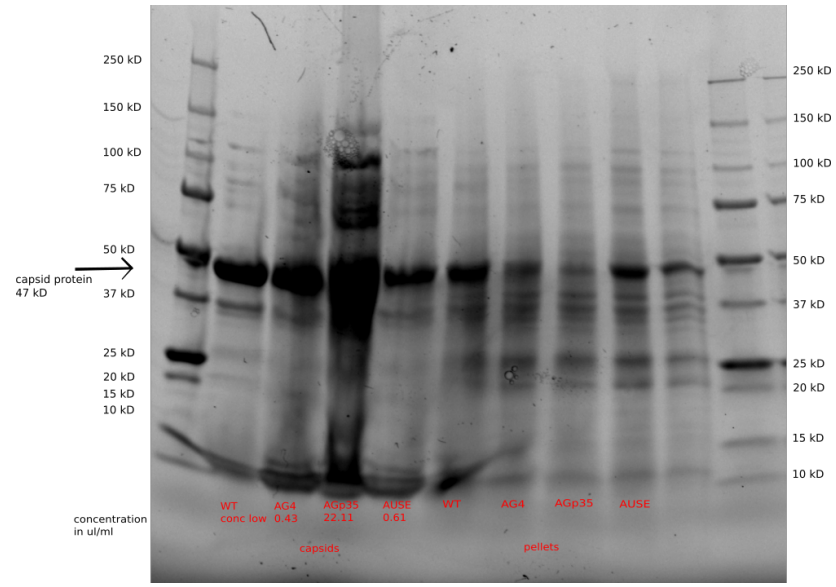

Figure R13: SDS-PAGE of P22 variants capsid solutions and pellets. The "pellet" samples were scrapings directly taken from the pelleted bacterial cultures and then boiled for 10 minutes at 95°C. The "capsids" samples were directly loaded from the extracted capsid solutions. P22 capsid protein subunits weigh 47 kDa and the SP_{141} weighs 18 kDa for the WT. The arrow indicates the capsid protein band.

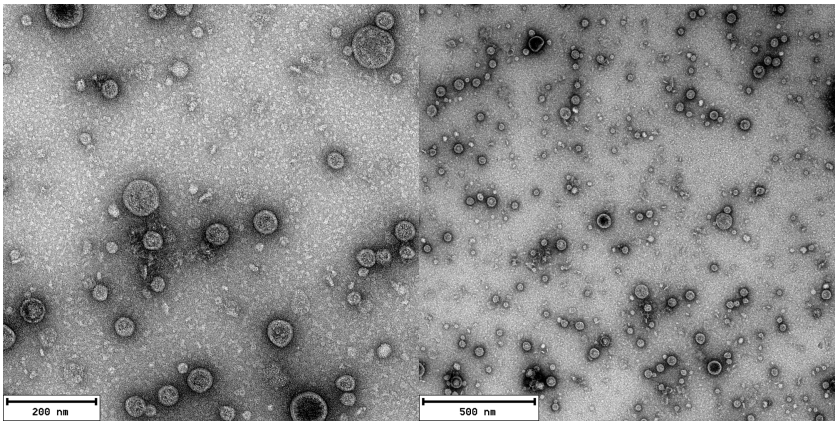

Figure R14: TEM images of the P22 WT capsids. The samples for TEM were prepared by Helena Shomar.

From the SDS-PAGE gels it can be seen that the capsid proteins are expressed in the BL21 cells for both our MS2 WT and P22 WT samples. For the P22 variants, the capsid protein can clearly be seen in all the pellets, but the band for the scaffold protein (expected at 18 to 20 kDa) cannot be identified. Although a band at approximately 22 kDa is seen, we cannot conclude this to be our scaffold protein band.

All the expressed capsid solutions show bands corresponding to our MS2 or P22 capsid proteins. The P22 AGP35 sample has a too high protein concentration, resulting in smudging of the gel, so for this sample we can't say for sure if the band is present. A vague band can be seen around 17 kDa for the P22 WT capsids sample from figure R12, which could correspond to our 18 kDa truncated scaffold protein. The MS2 bands are barely visible, suggesting low protein expression.

The TEM images show correct self-assembly of the P22 capsids. However, it can also be seen that the sample is very dirty. Therefore, the extracted capsids need to be purified using size-exclusion chromatography.

Because of the suspected low expression level of the MS2 monomers, we decided to clone it on a different backbone. Instead of the vector that was used before, it was decided to clone the MS2 constructs into the pET28a vector (see appendix 1). The commercial pET28a vector contains a T7 promoter instead of the lacUV5 promoter that was used before. The T7 promoter is a stronger promoter than the lacUV5 promoter, resulting in higher transcription and translation rates, leading to higher expression levels of the protein (Tegel, Ottosson, & Hober, 2011).

PURIFICATION OF THE CAPSIDS

The capsid solution of MS2 was purified via size-exclusion chromatography using the HiPrep 16/60 Sephacryl S-300 column on the AKTA. We obtained the chromatogram shown in figure R15b and fractions were collected of 2 mL each. Specific fractions for SDS-PAGE analysis were selected by comparing the obtained size-exclusion chromatography result to literature (figure R15a) (Tobias W. Giessen & Silver, 2016). As can be seen in the figure, we obtain similar results to the chromatograph by Giessen and Silver. As we don't know in which collected fractions our capsids are present, several fractions were selected over the range over the three visible peaks. The selected fractions were: fraction 9, 17, 21, 39, 41 and 45. These samples were run on an SDS-page gel (figure R16a), but unfortunately no bands were seen for any of the fractions. Considering that the absence of bands on the gel could be due to very low protein concentration in the fractions collected, we decided to concentrate the samples by a factor of 10 using Amicon Ultra 500 µL 3k centrifugal filter units. The concentrated samples were run on another SDS-PAGE gel. Unfortunately, we did not observe any specific protein band (figure R16b).

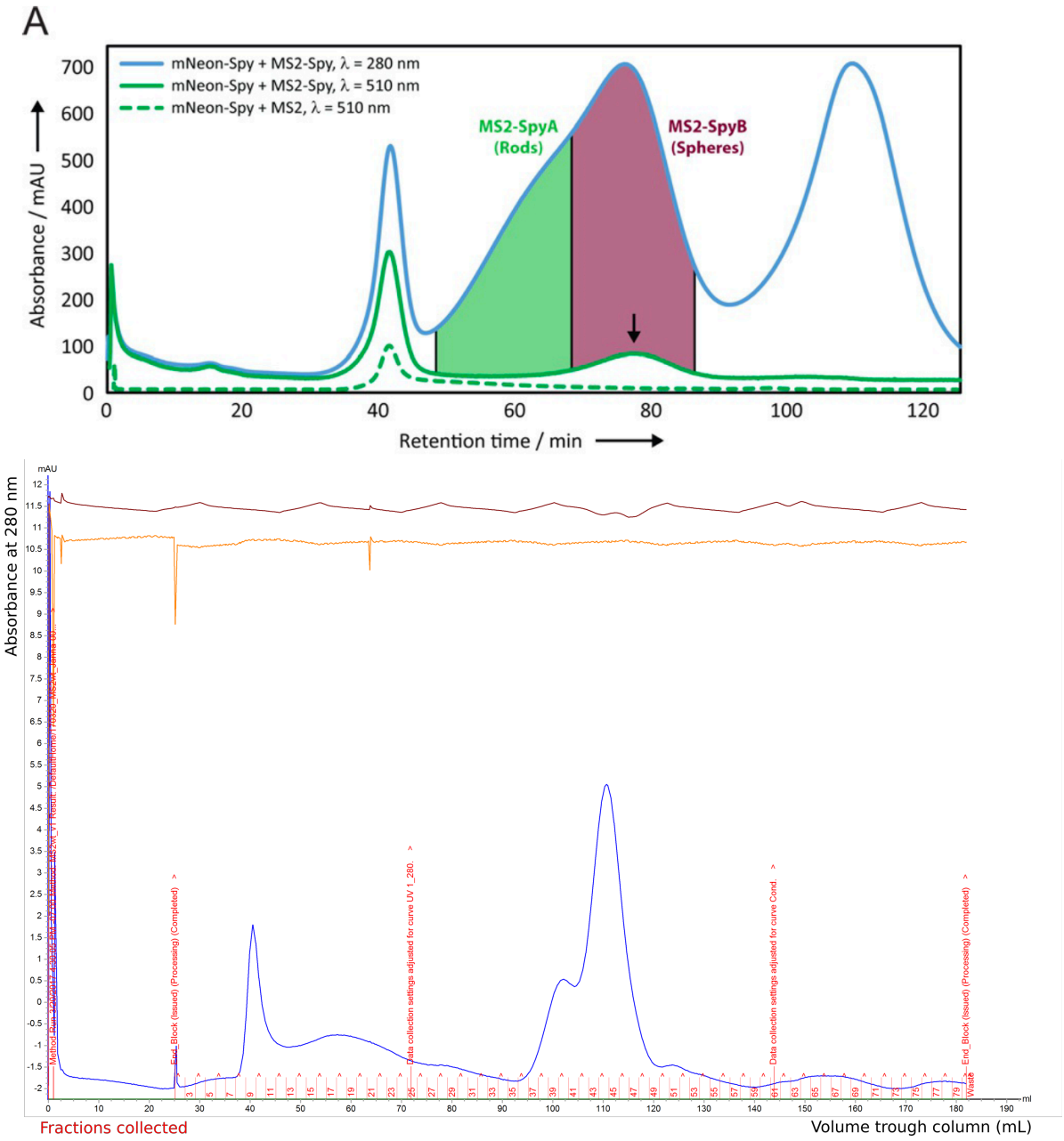

Figure R15: a) Size-exclusion chromatogram of the engineered and expressed MS2 capsids (Tobias W. Giessen & Silver, 2016), the MS2 capsids can be found in the red shaded area; b) Size-exclusion chromatogram of our MS2 WT capsids.

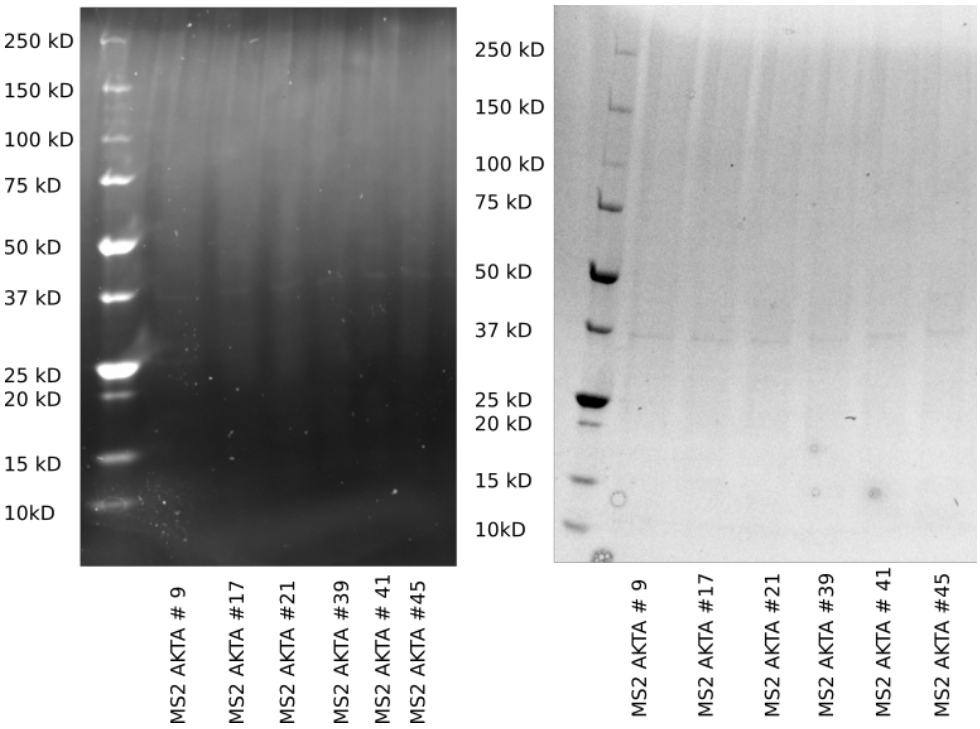

Figure R16: a) SDS-PAGE gel of MS2 samples after AKTA purification; b) SDS-PAGE gel of 10x concentrated MS2 samples after AKTA purification.

The MS2 sample loaded in the AKTA machine might have had a too low capsid concentration, as it was only purified from 50 mL of culture and resuspended in 3 mL of buffer. Because we are using a column with a volume of 120 mL, the capsid concentration in the collected fractions will be very low. Therefore, a second MS2 WT sample was run in AKTA (figure R17a), a sample derived from 200 mL of culture and resuspended in 1.5 mL of buffer. This should result in a more concentrated sample and might result in a nice peak on the chromatogram. A P22 WT sample, prepared with exactly the same steps, was also run in AKTA (figure R17b).

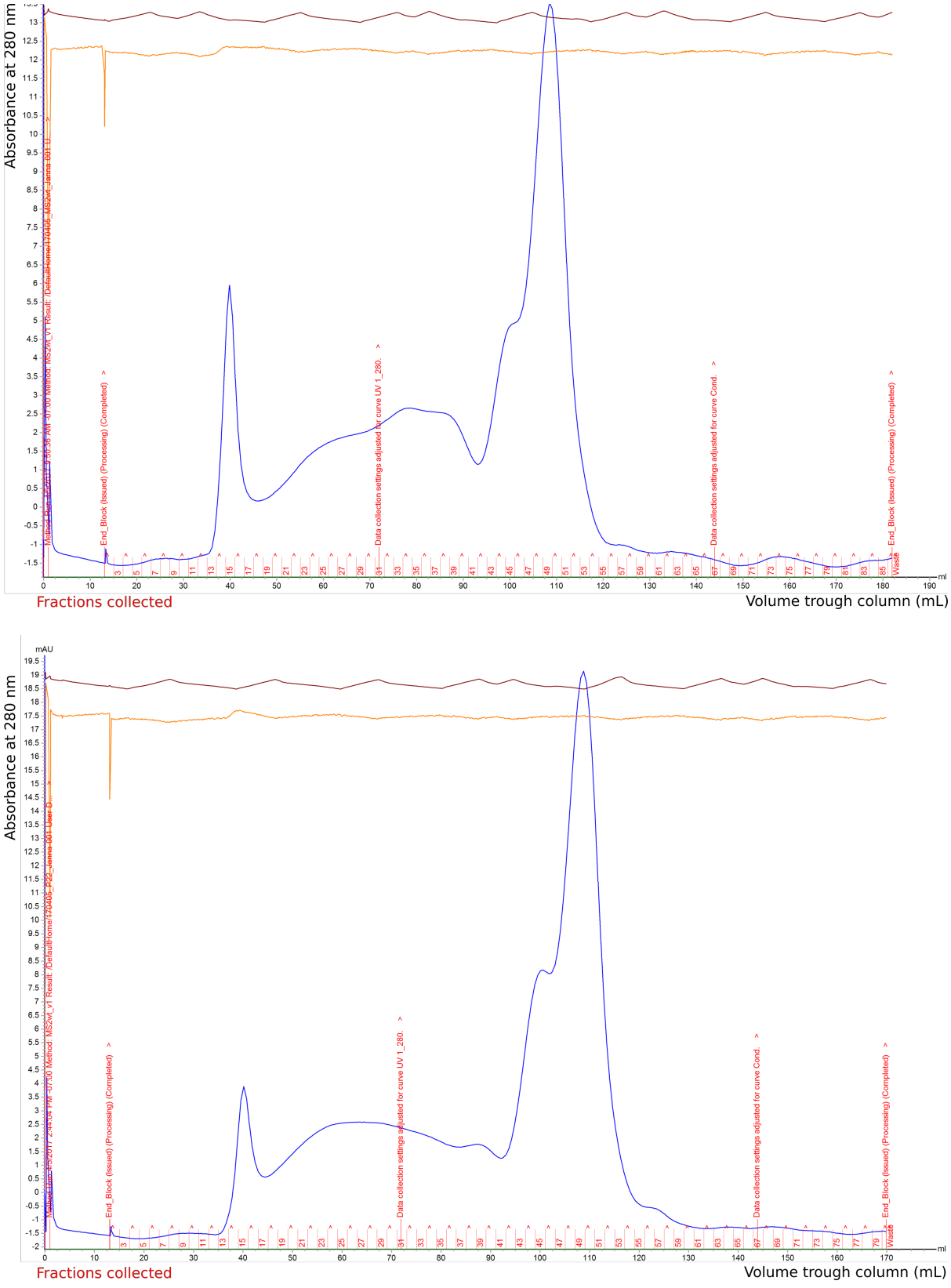

Figure R17: Size-exclusion chromatograms of MS2 WT (a; up) and P22 WT (b; down).

When compared to literature (figure R15a) and the first MS2 chromatogram (figure R15b), the resulting chromatograms (figure R17) show a larger peak at the expected site than the first MS2 chromatogram, but still show a significantly smaller peak than the chromatogram of Giessen and Silver. To detect in which

fractions the capsids could be found a selection of AKTA fractions was run on an SDS-PAGE gel (figure R18). The selected fractions were: P22 fractions 23, 27, 35 and 39; MS2 fractions 25, 34, 38 and 49.

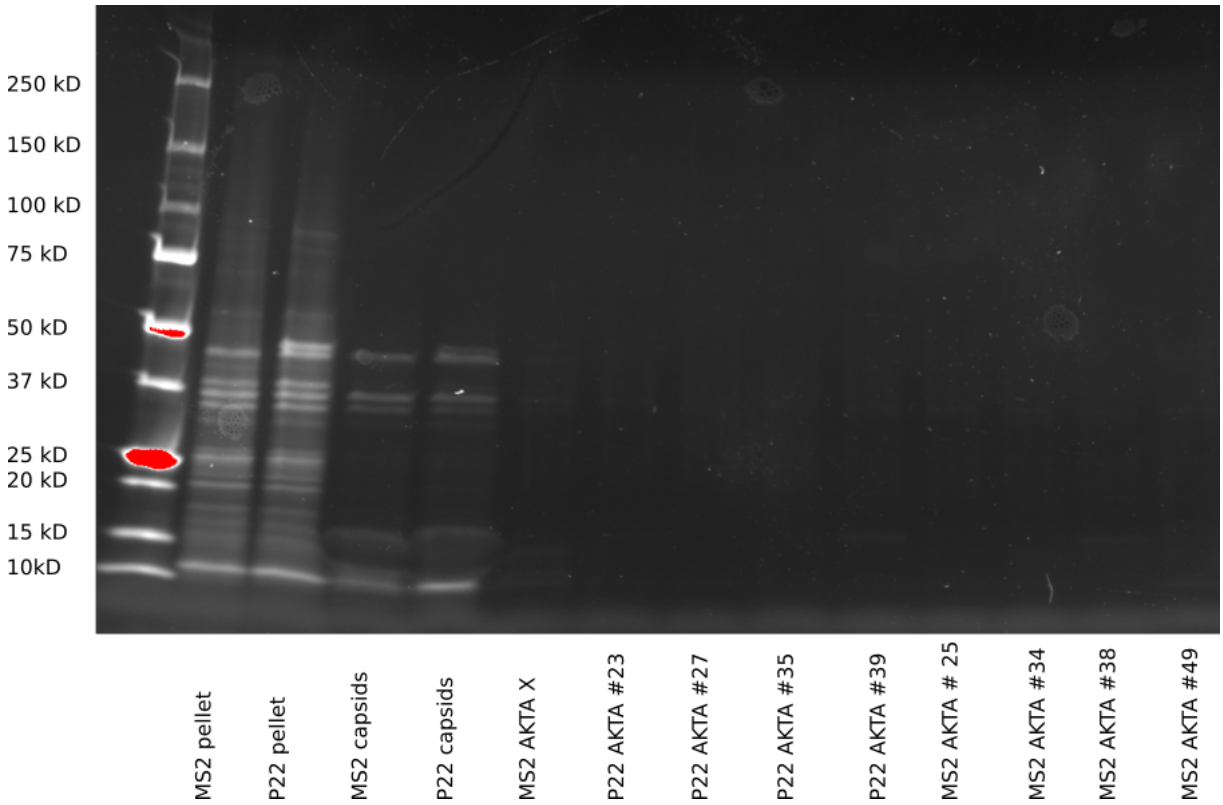

Figure R18: SDS-PAGE gel of selected AKTA fractions. The pellet and capsid samples, as well as the MS2 AKTA X can be disregarded.

No bands can be seen on the gel, leading to the conclusion that the samples are too diluted to see the capsids on the protein gel.

PRODUCTION OF NANOPARTICLES

In the scope and timeline of this thesis, we decided to conduct simple assay with unpurified capsids to test nanoparticle formation. The focus was put on silver nanoparticles, as one of the constructs for the gold nanoparticles wasn't correctly cloned yet.

We used two quick assays to determine whether nanoparticles were produced or not. The first assay was a cell extract assay, the second assay was a metal salt reduction assay.

CELL EXTRACT ASSAY

A cell extract is an in vitro transcription-translation system and consists of the content of a cell without the membrane proteins present. It can be used to express proteins directly without the need to lyse the cells before the proteins can be accessed. The cell extract used for this assay only needs linear DNA added to the cell extract mixture to initiate expression of the proteins. After the capsid monomers are expressed, we assume that capsids would self-assemble in the mixture as previously described in the literature (Garamella, Marshall, Rustad, & Noireaux, 2016). When metal salts are added, reduction of the metal salts by the peptides should commence and nanoparticles should be formed. We would be able to see this using UV-VIS spectroscopy, as the silver nanoparticles will show a peak in the UV-VIS spectrum.

To make the cell extract produce protein, the genes have to be under a T7 promoter. Without this promoter, transcription efficiency is very low in this system. To produce the linear DNA constructs containing the T7 promoter and capsid protein (and if applicable scaffold protein), Phusion PCR was performed. Primers were used that contained a tail with the T7 promoter on it. After purification of the DNA, it was added to the cell extract and the extract was incubated to express the capsid proteins. The expected capsid concentration after incubation is roughly between 1 and 10 µM. The next step was to add the metal salts; silver nitrate was added (in the dark) to the extracts to a final concentration of 100 mM. After incubation, the samples were diluted 2x, 10x and 50x, as the original reaction sample contained too much foam. The UV-VIS spectra for the wavelengths 230 nm to 700 nm were measured. The results can be seen in figures R19 and R20.

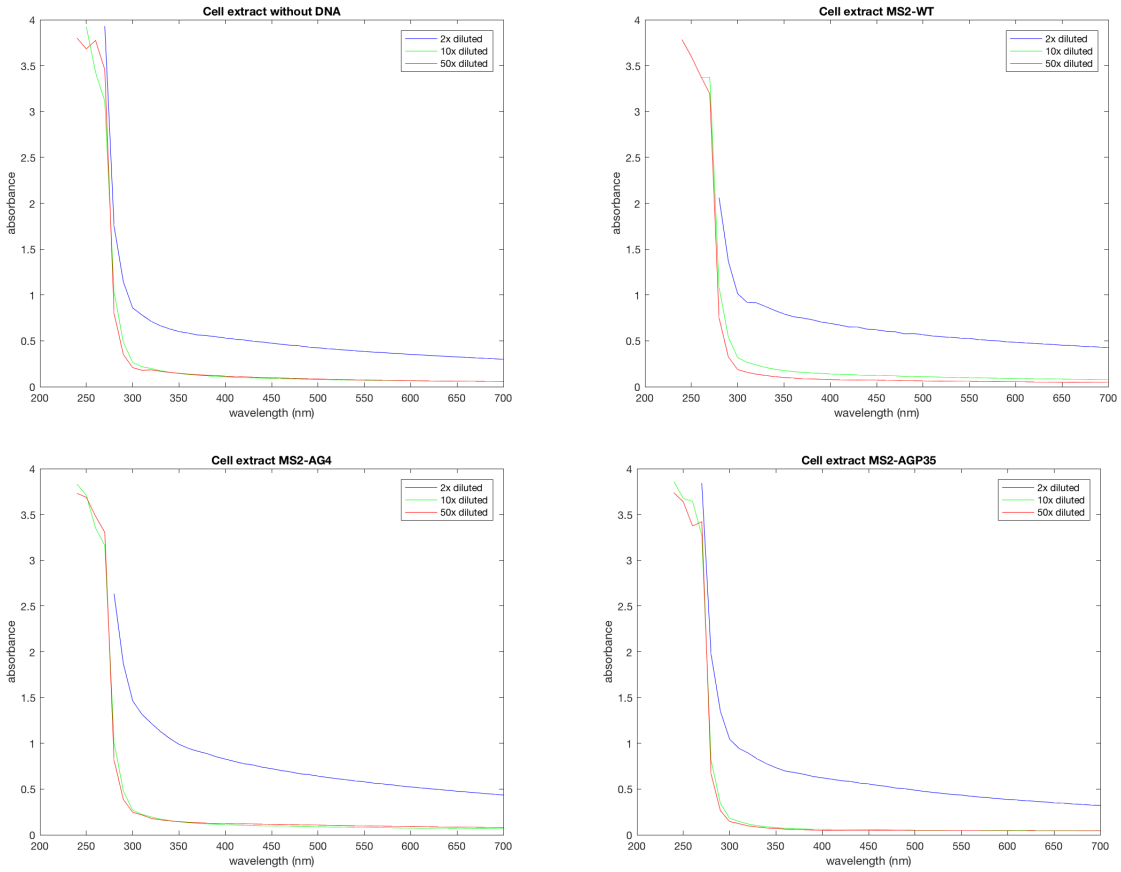

Figure R19: The UV-VIS spectra of the cell extract assay for the different MS2 constructs for silver nanoparticle formation. The cell extract without DNA was our negative control.

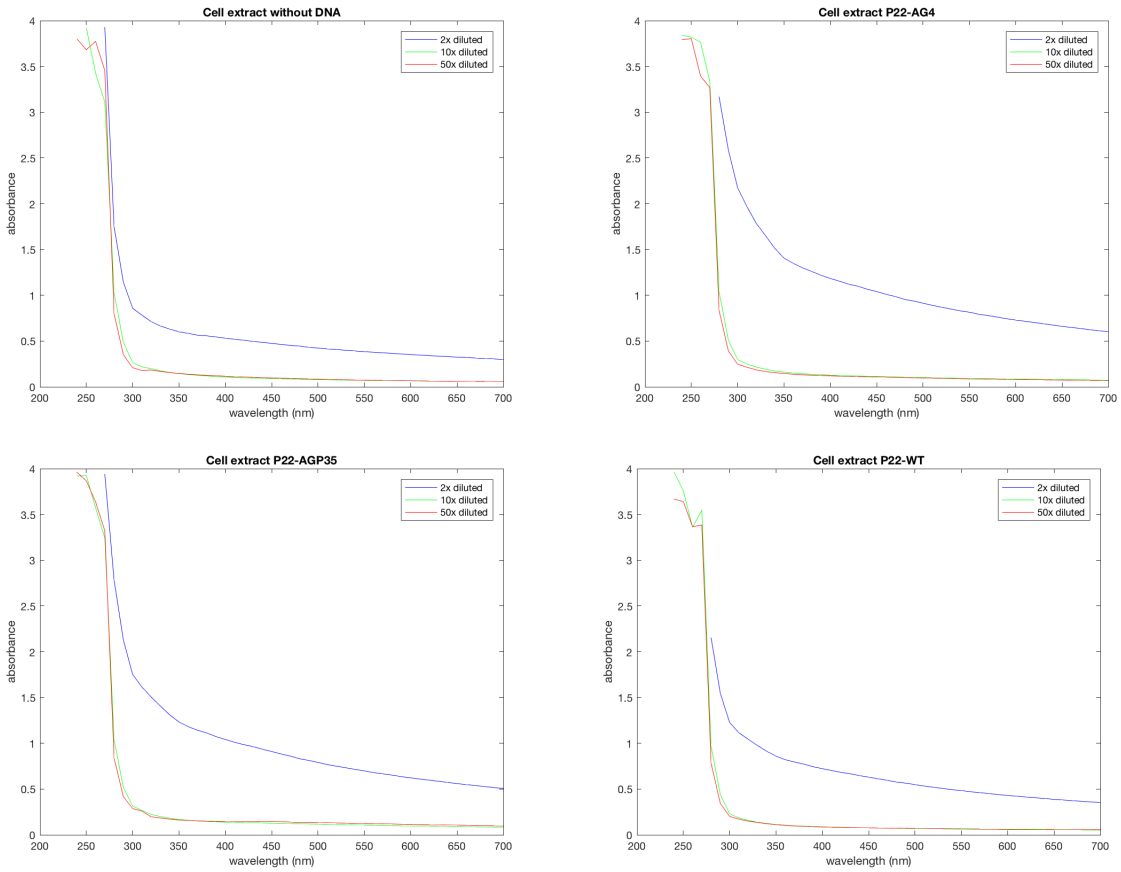

Figure R20: The UV-VIS spectra of the cell extract assay for the different P22 constructs for silver nanoparticle formation. The cell extract without DNA was our negative control.

The characteristic peak of the nanoparticles is not seen in the graphs, unfortunately. The UV-VIS spectra of the MS2 and P22 variants (WT, AG4 and AGP35 for each) didn't differ much from the negative control (the cell extract without DNA), suggesting that nanoparticle formation didn't take place.

Reason for the negative result might be that the expression of the capsid monomers was too low, as a too low expression of the monomers causes that the capsids don't self-assemble. This could for example be caused by the incubation step of the cell extract to express the monomers being too short (as it is incubated 6 hours, while in our capsid extraction protocol the cells are incubated for 18 hours).

It could also be that the expression of the monomer capsids was fine, but self-assembly into capsids did not occur. It could also be that the capsids were formed correctly and that nanoparticles were synthesized, but that the concentration of encapsulated nanoparticles was not high enough to cause a change in abosorbance and with that the detection of the nanoparticles using UV-VIS.

METAL SALT REDUCTION ASSAY

We decided to conduct an additional assay by using the extracted and precipitated capsid. This metal salt reduction assay would allow us to test if our extracted unpurified capsids synthesize nanoparticles. To a solution of extracted capsids in HEPES buffer, silver nitrate is added and the samples are incubated in the dark. If nanoparticles are synthesized by the engineered capsids, the UV-VIS spectrum will show an absorbance peak around 420 nm, the characteristic wavelength for 50 nm spherical silver nanoparticles. The two different sonication methods that were used for the extraction of the capsids, are also compared using this assay.

The assay uses four different metal salt concentrations (20 mM, 50 mM and 100 mM), which were based on similar work (Tobias Wolfgang Giessen & Silver, 2016). Protein concentrations of 10 µM and 1 µM were used, these concentrations were measured using the Bradford assay. All reactions occurred in HEPES buffer. As a negative control, HEPES buffer with the silver nitrate gradient was also taken into account. All reactions were performed in duplicates.

As mentioned in the methods section, the difference between method 1 and method 2 (see titles of the graphs) lies in the sonication process. Method 1 means sonication in 4 batches of 4 mL, while method 2 means sonication in a batch of 16 mL. We wanted to compare sonication methods as the sonication of larger volumes is necessary for the scaling up of the process.

For the assay the P22 samples were used, as the MS2 samples have a too low concentration, as previously shown. The capsids P22 WT, P22 AG4 and P22 AGP35 were used; as negative control empty BL21 cells without plasmid were used. The empty BL21 cells were processed using the same steps as the BL21 cells containing the plasmids for the capsids. HEPES buffer with the different salt concentrations was used to verify whether the salt gradient had any influence on the absorbance spectrum. The resulting UV-VIS spectra of the assay can be found in figures R21 to R24.

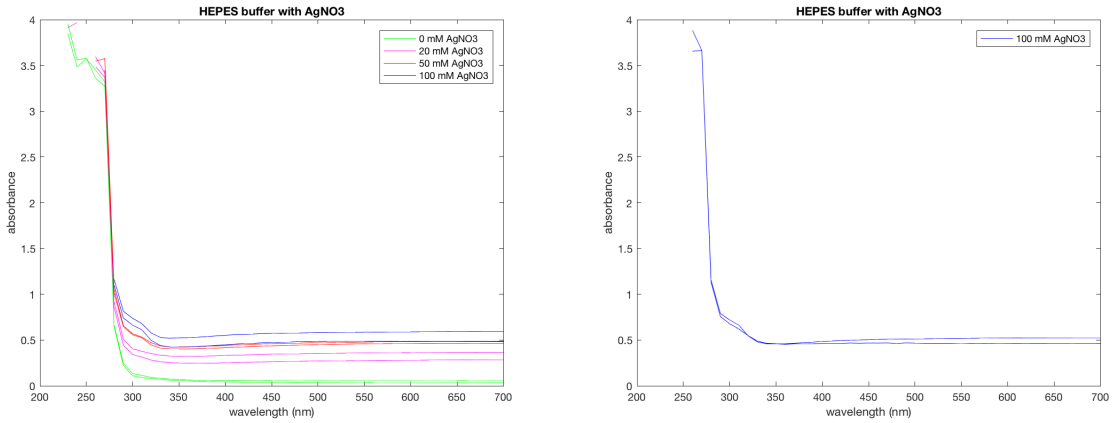

Figure R21: UV-VIS spectra of the HEPES buffer with different concentrations of silver nitrate added.

From the UV-VIS spectra of the HEPES buffer alone with silver nitrate, we can see that the salt concentration has a small effect on the absorbance spectrum of the sample. However, the absorbance levels are constant over the range of the wavelengths, which shows us that no nanoparticles are formed, as expected.

The UV-VIS spectrum of P22 AG4 (figure R22) shows no sign of nanoparticle formation. There is no absorbance peak around 420 nm. It would have been better if the 100 mM concentration was tested with a lower concentration of capsids (1 µM instead of 10 µM) as well, as was done with the AGP35 samples. When comparing the spectrum of AG4 with the BL21 empty method 1 graph of the same concentration (figure R23), they look very similar, which is in line with our conclusion that no nanoparticles are synthesized.

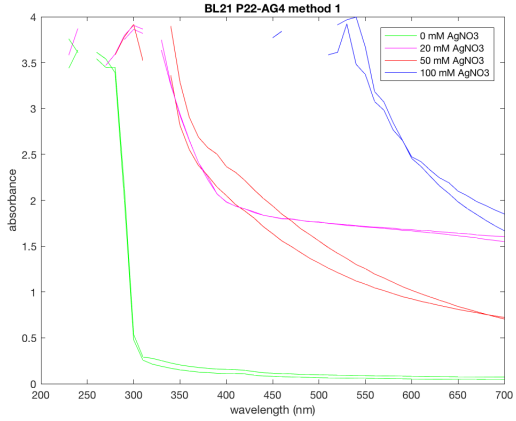

Figure R22: The UV-VIS spectrum of P22 AG4.

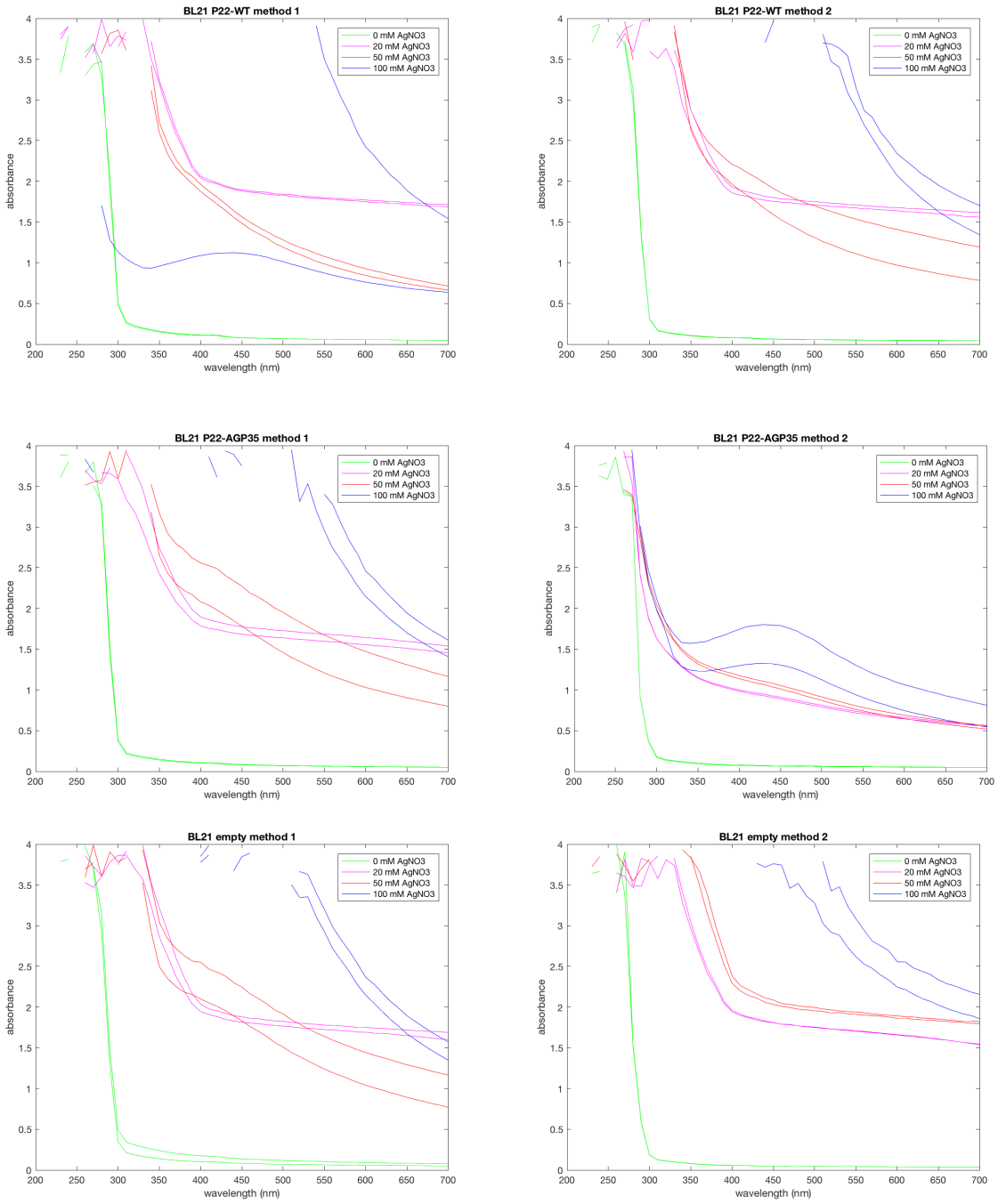

Figure R23: P22 WT, P22 AGP35 and BL21 empty UV-VIS spectra for multiple salt concentrations and a protein concentration of 10 µM. The lower blue line in the P22 WT spectrum, corresponding to a salt concentration of 100 mM, was incorrect as there was not enough extracted capsid sample to perform the assay with.

From the first experiment performed, the range of silver nitrate concentrations was tested for the P22 AG4 capsids (as mentioned above), the P22 WT and the P22 AGP35 capsids and the empty BL21 samples. With this experiment sonication methods could also be compared. The results of this assay can be found in figure R23.

Only one sample shows an absorbance peak characteristic for the silver nanoparticles at 420 nm. This is the P22 AGP35 sample that was sonicated in a large batch with a silver nitrate concentration of 100 mM. As the other samples with 100 mM silver nitrate showed a too high absorbance to detect for a large range of

wavelengths, we suspected this might be caused by a too high capsid concentration. Therefore, the assay was run again with a protein concentration of 1 µM instead of 10 µM. The samples AGP35 and BL21 empty were used for this second assay, as one of the P22 WT samples was finished. The results of this experiment are shown in figure R24.

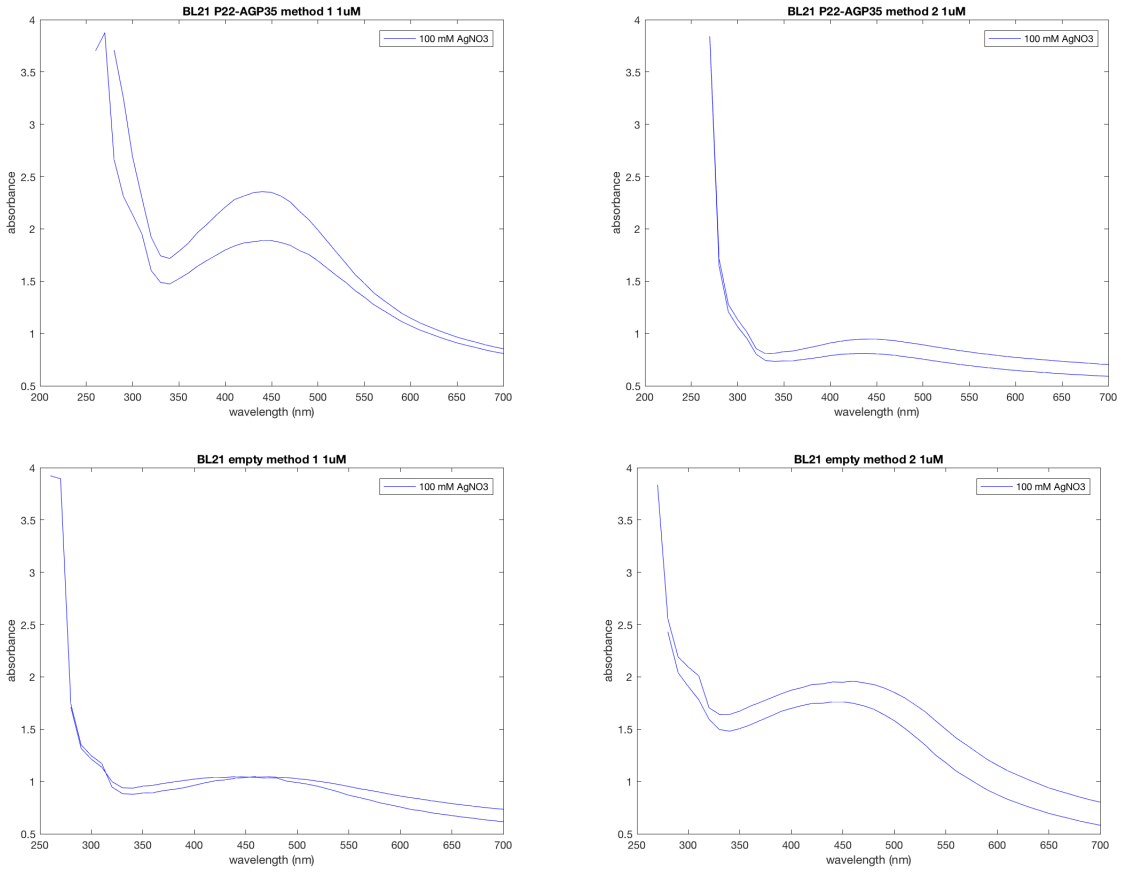

Figure R24: UV-VIS spectra of BL21 empty samples and P22 AGP35 capsids. Only one concentration of silver nitrate was used, 100 mM. The protein concentration used was 1 µM.

The new UV-VIS spectra gave us more insight into the differences between the sonication methods and showed the absorbance of the samples around the characteristic absorbance wavelength of silver nanoparticles better, which is at 420 nm. We see a high absorbance peak around 420 nm in the P22 AGP35 method 1 sample, indicating the presence of nanoparticles. Comparing this to the spectrum of the BL21 empty method 1, a large difference is seen. In the BL21 empty method 1 sample, no nanoparticles were formed. However, if we look at the method 2 samples, the results are confusing. In the AGP35 method 2 graph, we can see that there is a too low concentration of nanoparticles to detect the or that there are no nanoparticles present in the sample, contradicting the results we obtained from the same sample in the first experiment (figure R23). A probable explanation for this is that the AGP35 capsids did synthesize nanoparticles, but that the capsid concentration was too low when 1 µM of protein was used. This could be the case because sonication method 2 could be worse at lysing the cells, leaving more cell debris and other unwanted components behind compared to method 1, resulting in a higher protein concentration of which a smaller percentage is capsids.

The absence of the characteristic absorbance peak could be explained for the P22 AGP35 sample, but the presence of an absorbance peak in the BL21 empty method 2 cells is harder to explain. It could be that

because of the sonication method used (method 2), which we think is less effective at lysing the cells, more cell membrane debris and with that protein was left in the sample. As mentioned before, some membrane proteins of *E. coli* can synthesize nanoparticles and this could be the peak that was seen.

Considering the different sonication methods, it is not clear what influence the sonication method has on the samples. We have theorized about this, but not much is known about the influence of the sonication on the reducing capabilities of the capsids.

The results are inconclusive, which is a shame, as the assay looked promising when the colors of the samples were studied by eye (figure R25). The BL21 samples show large chunks of aggregated silver nitrate, while the AGP35 samples show less chunks, but do show a red color. As a red color is characteristic for silver nanoparticles of a size around 100 nm, it could mean that the nanoparticles are produced, as the AGP35 samples show a darker (method 1) or lighter (method 2) red color.

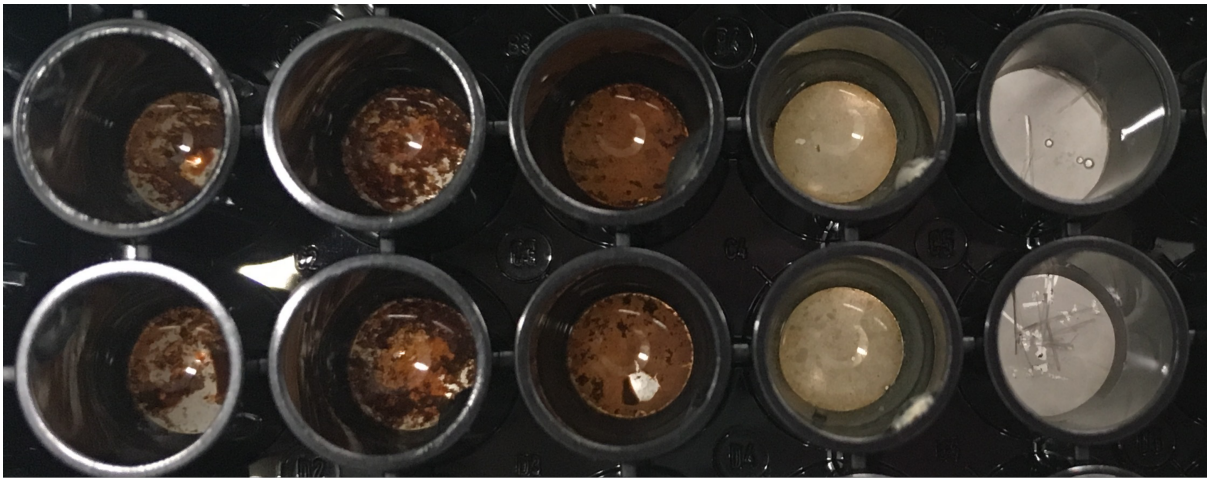

Figure R25: Picture of the samples of the second metal salt assay experiment.

The results would have been able to tell us more if the capsid samples had been purified. The purification is an important step that we unfortunately couldn't do successfully.

DISCUSSION

The goal of the project was to produce silver and golden nanoparticles within engineered protein scaffolds using reducing peptides. To this end, appropriate peptides and viral capsids were selected from literature. The monomers of MS2 were modeled and the most promising constructs were chosen to clone. In P22, the peptides were successfully fused to the interior of the capsids, without influencing the self-assembling ability of the capsids. For MS2, the peptides were integrated in the monomers of the capsid, but self-assembly hasn't been shown yet. The production of nanoparticles in our engineered P22 and MS2 capsids was not confirmed, as the results were inconclusive.

In this thesis the project was limited in several ways. Time was of course a big factor, as the time set for a BSc thesis is only six months. Within cloning the P22 AURW was never successfully cloned, limiting the experiments we could do to only silver nanoparticle production. The pET MS2 constructs encountered the same problem, it took weeks to clone the MS2 constructs into the pET vector, while this could have been done in a few days. Although the cloning failing was my fault (as I found out at a certain point in time, the first try after I found out the cloning was successful), it did cost me a lot of time that I could have spent on the assays to test for nanoparticle production. Within the capsid expression process, a limitation was that scaling up the capsid extraction did not work and we therefore needed to invest extra time in creating multiple samples.

But the biggest limitation was found in being unable to purify the capsids, as we do not know the composition of our samples at the moment. This is also directly where we can make the biggest improvement. At the moment the samples are possibly contaminated with other proteins, such as the membrane proteins that have been shown to reduce metal salts to metallic nanoparticles or cell debris that weren't properly removed from the sample. This influences the results and makes it impossible to verify with certainty if our engineered capsids can synthesize nanoparticles. To do the purification, AKTA is still the best solution, as it is a widely used machine for protein purifications and has been shown to successfully isolate the capsids based on their size by other researchers.

Another improvement would if the pET vector increases the concentration of the expressed capsids. This should be tested by expressing the pET MS2 plasmids in BL21 cells and look at the resulting protein concentration. If the concentration is significantly higher, the samples might even be used for purification using the AKTA and can certainly be used for a metal reduction assay with gold ions.

The future of this project could lie in using cell extracts for the synthesis of encapsulated metallic nanoparticles for all sorts of applications. The idea would be to produce nanoparticles within a protein cage that can be easily decorated on the outside by a simple genetic modification. The ideal implementation would be a plug-and-play nanoreactor for which the material and size of the nanoparticle and the components displayed on the outside of the protein cage can be selected using a prefabricated modular genetic system. If this could be made, the nanoreactors might also be taken outside the lab, or at least there will be no need anymore for the high-tech equipment that needs to be used for capsid extraction from bacteria.

ACKNOWLEDGEMENTS

First of all, I would like to thank dr. Greg Bokinsky for offering me this amazing project, keeping my goals clear and helping me chase down my parcels with DNA.

A very big thank you to Helena Shomar Monges, without whom my thesis wouldn't have been possible at all. She has supervised my everyday work and helped me out whenever I needed it. Because of her, I've learned to work independently in the lab and think every step trough. Hopefully she can continue this project and will my work on cloning the constructs help her on her way.

Special thanks to David Foschepoth for providing me with cell extracts that I could use for my experiment and for answering the many questions I had about working with the extract.

Thanks to dr. Marie-Eve Aubin-Tam for agreeing on being my second examiner.

I would also like to thank all (former) members of the Bokinsky group for the help, the advice, the nice chats and the warm welcome.

Finally, I want to thank my family and friends for all the mental support and the positive vibes, you helped me put my focus where it belonged: on my project.

The protein models were visualized using the UCSF Chimera package. Chimera is developed by the Resource for Biocomputing, Visualization, and Informatics at the University of California, San Francisco (supported by NIGMS P41-GM103311).

REFERENCES

Akbari, B., Tavandashti, M. P., & Zandrahimi, M. (2011). Particle Size Characterization of Nanoparticles - A practical approach, *8*(2), 48–56.

Bae, D.-S., Kim, E.-J., Bang, J.-H., Kim, S.-W., Han, K.-S., Lee, J.-K., … Adair, J. H. (2005). Synthesis and characterization of silver nanoparticles by a reverse micelle process. *Metals and Materials International*, *11*(4), 291–294. https://doi.org/10.1007/BF03027331

Binnig, G., & Quate, C. (1986). Atomic Force Microscope. *Physical Review Letters*, *56*(9), 930–33.

Binnig, G., & Rohrer, H. (1983). Scanning Tunneling Microscopy, *126*, 236–244.

Brown, S., Sarikaya, M., & Johnson, E. (2000). A genetic analysis of crystal growth. *Journal of Molecular Biology*, *299*(3), 725–735. https://doi.org/10.1006/jmbi.2000.3682

Burda, C., Chen, X., Narayanan, R., & El-Sayed, M. A. (2005). Chemistry and properties of nanocrystals of different shapes. *Chemical Reviews*. https://doi.org/10.1021/cr030063a

Cho, K., Wang, X., Nie, S., Chen, Z., & Shin, D. M. (2008). Therapeutic nanoparticles for drug delivery in cancer. *Clinical Cancer Research*, *14*(5), 1310–1316. https://doi.org/10.1158/1078-0432.CCR-07-1441

Chou, L. Y. T., Ming, K., & Chan, W. C. W. (2011). Strategies for the intracellular delivery of nanoparticles. *Chem. Soc. Rev.*, *40*(1), 233–245. https://doi.org/10.1039/C0CS00003E

Dickerson, M. B., Sandhage, K. H., & Naik, R. R. (2008). Protein- and peptide-directed syntheses of inorganic materials. *Chemical Reviews*, *108*(11), 4935–4978. https://doi.org/10.1021/cr8002328

Douglas, T., Strable, E., Willits, D., Aitouchen, A., Libera, M., & Young, M. (2002). Protein engineering of a viral cage for constrained nanomaterials synthesis. *Advanced Materials*, *14*(6), 415–418. https://doi.org/10.1002/1521-4095(20020318)14:6<415::AID-ADMA415>3.0.CO;2-W

Dragomir, M. (n.d.). METALLIC NANOPARTICLES, 1–50.

Duncan, T. V. (2014). Applications of nanotechnology in food packaging and food safety : Barrier materials , antimicrobials and sensors. *JOURNAL OF COLLOID AND INTERFACE SCIENCE*, (2011). https://doi.org/10.1016/j.jcis.2011.07.017

Feynman, R. (1957). There ' s Plenty of Room at the Bottom.

Garamella, J., Marshall, R., Rustad, M., & Noireaux, V. (2016). The All E. coli TX-TL Toolbox 2.0: A Platform for Cell-Free Synthetic Biology. *ACS Synthetic Biology*, *5*(4), 344–355. https://doi.org/10.1021/acssynbio.5b00296

Garcia, M. A. (2011). Surface plasmons in metallic nanoparticles : fundamentals and applications To cite this version : Surface Plasmons in metallic nanoparticles : Fundamentals and.

Giessen, T. W., & Silver, P. A. (2016). A Catalytic Nanoreactor Based on in Vivo Encapsulation of Multiple Enzymes in an Engineered Protein Nanocompartment. *ChemBioChem*, *17*(20), 1931–1935. https://doi.org/10.1002/cbic.201600431

Giessen, T. W., & Silver, P. A. (2016). Converting a natural protein compartment into a nanofactory for the size-constrained synthesis of antimicrobial silver nanoparticles. *ACS Synthetic Biology*, acssynbio.6b00117. https://doi.org/10.1021/acssynbio.6b00117

Han, G., Ghosh, P., & Rotello, V. M. (2007). Functionalized gold nanoparticles for drug delivery. *Nanomedicine*, *2*(1), 113–23.

Iravani, S., Korbekandi, H., Mirmohammadi, S., & Zolfaghari, B. (2014). Synthesis of silver nanoparticles: chemical, physical and biological methods. *Research in Parmaceutical Sciences*, *9*(6), 385–406.

Kelley, L. A., Mezulis, S., Yates, C. M., Wass, M. N., & Sternberg, M. J. E. (2015). The Phyre2 web portal for protein modeling, prediction and analysis. *Nat. Protocols*, *10*(6), 845–858. Retrieved from http://dx.doi.org/10.1038/nprot.2015.053

Kelly, K. L., Coronado, E., Zhao, L. L., & Schatz, G. C. (2003). The optical properties of metal nanoparticles: The influence of size, shape, and dielectric environment. *Journal of Physical Chemistry B*, *107*(3), 668–677. https://doi.org/10.1021/jp026731y

Li, X., Xu, H., Chen, Z. S., & Chen, G. (2011). Biosynthesis of nanoparticles by microorganisms and their applications. *Journal of Nanomaterials*. https://doi.org/10.1155/2011/270974

Link, S., & El-Sayed, M. A. (1999). Size and Temperature Dependence of the Plasmon Absorption of Colloidal Gold Nanoparticles. *The Journal of Physical Chemistry B*, *103*(21), 4212–4217. https://doi.org/10.1021/jp9847960

Lovley, D. R. (1991). Magnetite Formation During Microbial Dissimilatory Iron Reduction. In R. B. Frankel & R. P. Blakemore (Eds.), *Iron Biominerals* (pp. 151–166). Boston, MA: Springer US. https://doi.org/10.1007/978-1-4615-3810-3_11

Milligan, W. O., & Morriss, R. H. (1964). Morphology of Colloidal Gold - A comparative Study. *J. Am. Chem. Soc.*, *86*(17), 3461–3467.
Naik, R. R., Jones, S. E., Murray, C. J., McAuliffe, J. C., Vaia, R. A., & Stone, M. O. (2004). Peptide Templates for Nanoparticle Synthesis Derived from Polymerase Chain Reaction-Driven Phage Display. *Advanced Functional Materials*, *14*(1), 25–30. https://doi.org/10.1002/adfm.200304501
Naik, R. R., Stringer, S. J., Agarwal, G., Jones, S. E., & Stone, M. O. (2002). Biomimetic synthesis and patterning of silver nanoparticles. *Nature Materials*, *1*(3), 169–72. https://doi.org/http://dx.doi.org/10.1038/nmat758
NSTC. (2007). The National Technology Initiative - Strategic Plan. *Executive Office of the President of the United States*.
Ostro, M., & Cullis, P. (1989). Use of liposomes as injectable-drug delivery systems. *Am J Hosp Pharm.*, *46*(8), 1576–87.
Parker, M., Casjens, S., & Prevelige, P. (1998). Functional domains of bacteriophage P22 scaffolding protein. *J Mol Biol*, *281*(1), 69–79.
Patungwasa, W., & Hodak, J. H. (2008). pH tunable morphology of the gold nanoparticles produced by citrate reduction. *Materials Chemistry and Physics*, *108*(1), 45–54.
Pettersen, E. F., Goddard, T. D., Huang, C. C., Couch, G. S., Greenblatt, D. M., Meng, E. C., & Ferrin, T. E. (2004). UCSF Chimera - a visualization system for exploratory research and analysis. *J Comput Chem*, *25*(13), 1605–12.
Qu, X., Alvarez, P. J. J., & Li, Q. (2013). Applications of nanotechnology in water and wastewater treatment. *Water Research*, *47*(12), 3931–3946. https://doi.org/10.1016/j.watres.2012.09.058
Quester, K., Avalos-Borja, M., & Castro-Longoria, E. (2013). Biosynthesis and microscopic study of metallic nanoparticles. *Micron*, *54–55*, 1–27. https://doi.org/10.1016/j.micron.2013.07.003
Reichhardt, C., Uchida, M., O'Neil, A., Li, R., Prevelige, P. E., & Douglas, T. (2011). Templated assembly of organic-inorganic materials using the core shell structure of the P22 bacteriophage. *Chemical Communications (Cambridge, England)*, *47*(22), 6326–6328. https://doi.org/10.1039/c1cc11215e
Said, J., Dodoo, C. C., Walker, M., Parsons, D., Stapleton, P., Beezer, A. E., & Gaisford, S. (2014). An in vitro test of the efficacy of silver-containing wound dressings against Staphylococcus aureus and Pseudomonas aeruginosa in simulated wound fluid. *International Journal of Pharmaceutics*, *462*(1–2), 123–128. https://doi.org/10.1016/j.ijpharm.2013.12.037
Sanchez, F., & Sobolev, K. (2010). Nanotechnology in concrete - A review. *Construction and Building Materials*, *24*(11), 2060–2071. https://doi.org/10.1016/j.conbuildmat.2010.03.014
Schwarz, B., Madden, P., Avera, J., Gordon, B., Larson, K., Miettinen, H. M., … Douglas, T. (2015). Symmetry Controlled, Genetic Presentation of Bioactive Proteins on the P22 Virus-like Particle Using an External Decoration Protein. *ACS Nano*, *9*(9), 9134–9147. https://doi.org/10.1016/j.bbamem.2015.02.010.Cationic
Srivastava, S. K., Yamada, R., Ogino, C., & Kondo, A. (2013). Biogenic synthesis and characterization of gold nanoparticles by Escherichia coli K12 and its heterogeneous catalysis in degradation of 4-nitrophenol. *Nanoscale Research Letters*, *8*(1), 70. https://doi.org/10.1186/1556-276X-8-70
Tan, Y. N., Lee, J. Y., & Wang, D. I. C. (2010). Uncovering the Design Rules for Peptide Synthesis of Metal Nanoparticles. *Journal of the American Chemical Society*, *132*(16), 5677–5686. https://doi.org/Doi 10.1021/Ja907454f
Tegel, H., Ottosson, J., & Hober, S. (2011). Enhancing the protein production levels in Escherichia coli with a strong promoter. *FEBS Journal*, *278*(5), 729–739. https://doi.org/10.1111/j.1742-4658.2010.07991.x
Tsuzuki, T. (2009). Commercial scale production of inorganic nanoparticles. *International Journal of Nanotechnology*, *6*(5/6), 567. https://doi.org/10.1504/IJNT.2009.024647
Zhang, Y., Werling, U., & Edelmann, W. (2012). SLiCE : a novel bacterial cell extract-based DNA cloning method, *40*(8), 1–10. https://doi.org/10.1093/nar/gkr1288
Zhao, G., & Stevens, S. J. (1998). Multiple parameters for the comprehensive evaluation of the susceptibility of Escherichia coli to the silver ion. *Biometals*, *11*(1), 27–32.

Extra references used (current as of July 5th 2017):

1. List of Nanotechnology applications - http://bionanotech.uniss.it/?p=760
2. Sigma-Aldrich Internet Catalogue - http://www.sigmaaldrich.com/materials-science/material-science-products.html?TablePage=16376744

3. What's so special about the nanoscale? - https://www.nano.gov/nanotech-101/special
4. Codon optimization IDT dna - https://eu.idtdna.com/CodonOpt
5. Geneious version 9.1 created by Biomatters. Available from http://www.geneious.com
6. Nanoparticles of different sizes emit different coloured light - https://i.stack.imgur.com/irMiu.png
7. Chemical reduction of gold nanoparticles - http://sustainable-nano.com/2014/06/10/two-ways-to-make-nanoparticles/

APPENDIX 1

pMS2 PLASMIDS

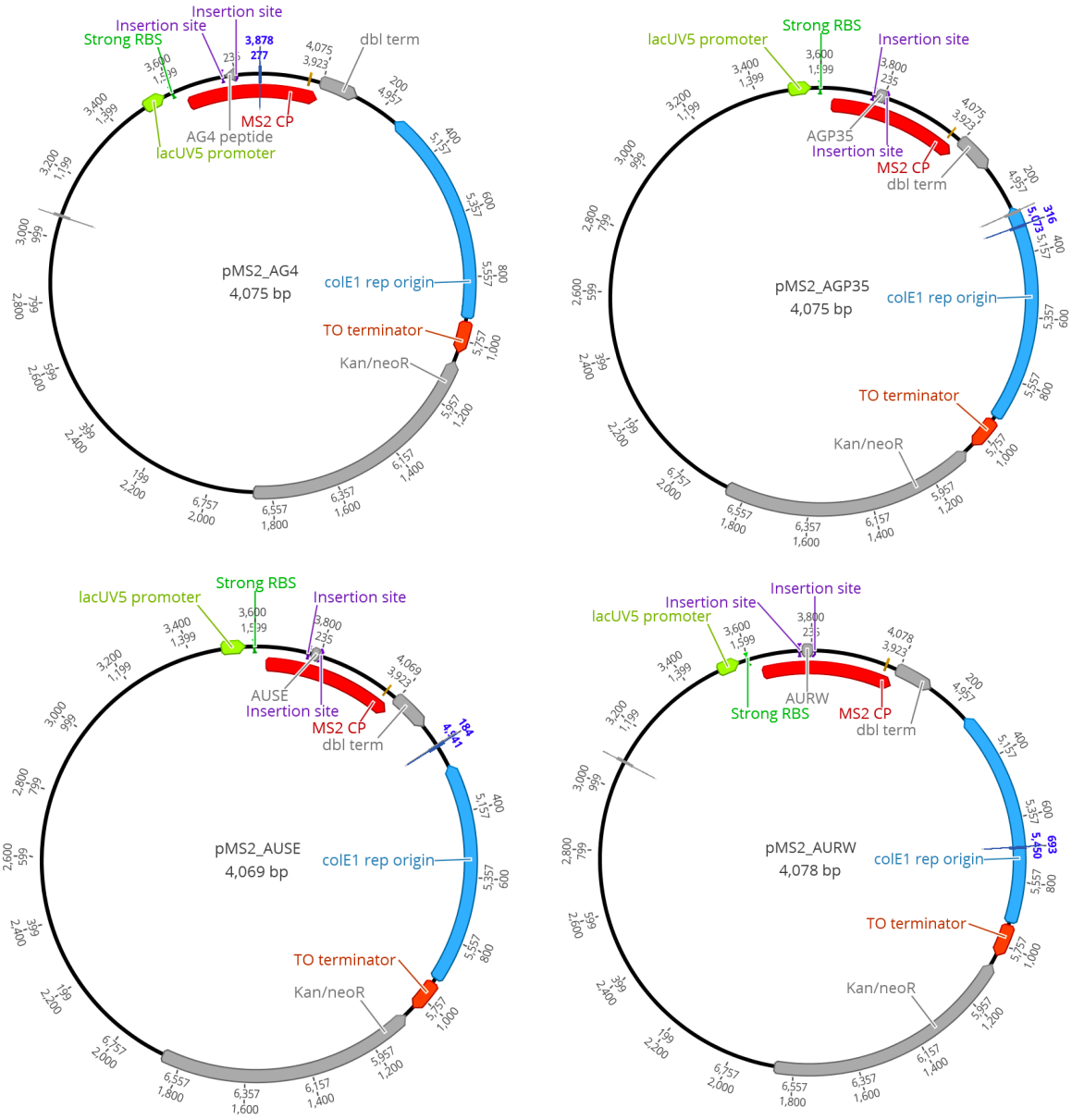

Figure A1: Plasmid maps of the MS2 constructs. pMS2_WT can be found in the results section.

pP22 PLASMIDS

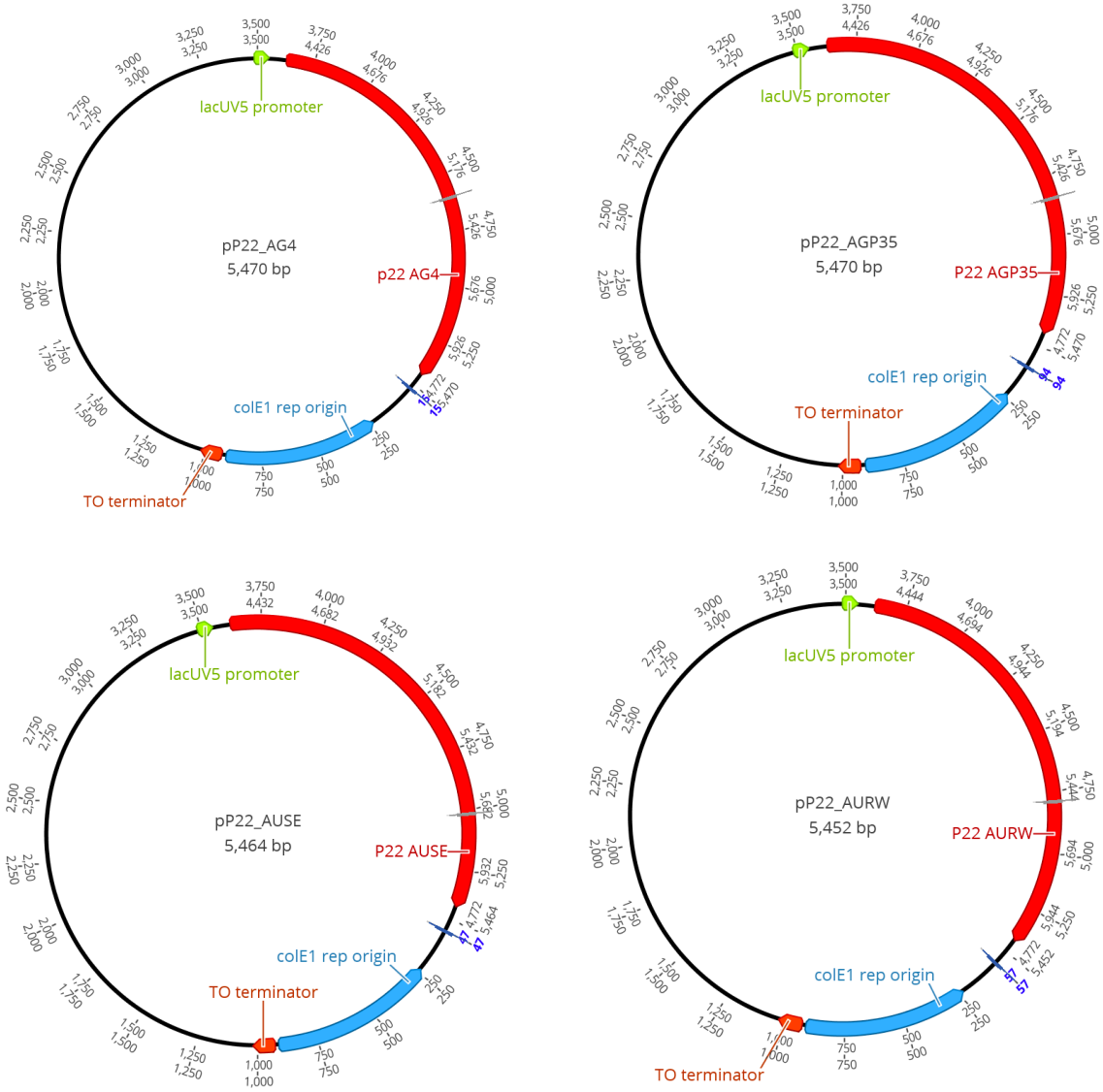

Figure A2: Plasmid maps of the P22 constructs. pP22_WT can be found in the results section.

pETMS2 PLASMIDS

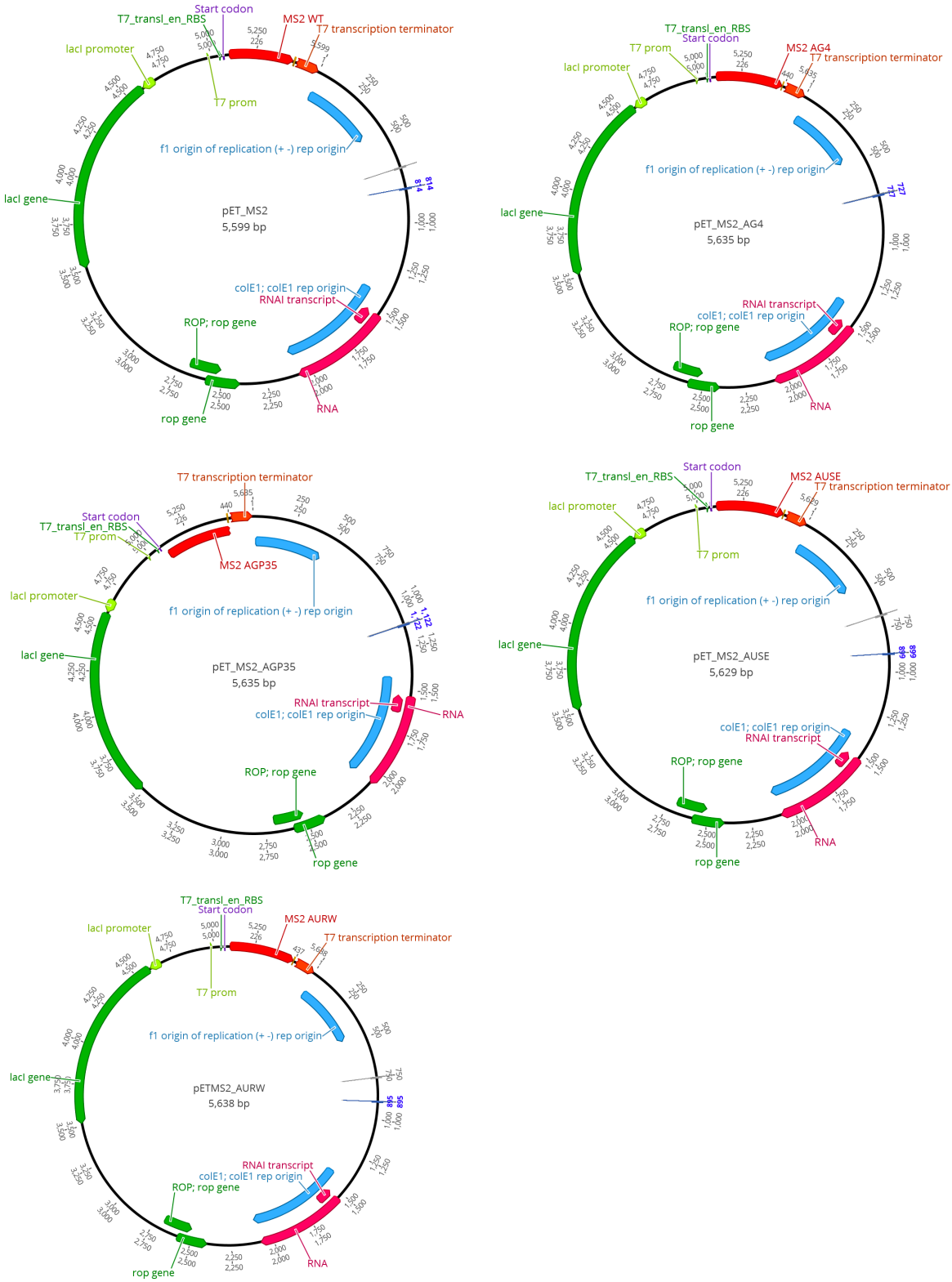

Figure A3: Plasmid maps of the MS2 constructs in the pET vector.

APPENDIX 2

LIST OF ALL USED PRIMERS

Name	Sequence
HS318_pET vector R	CATGGTATATCTCCTTCTTAAAGTTAAACAAAATTATTTCTAGAGGGGAATTGTTATCC
HS317_pET vector F	TGAGATCCGGCTGCTAACAAAGCCCGAAAGGAAGCTGAGTTGGCTGCTG
HS316_MS2 pET R	CTTTCGGGCTTTGTTAGCAGCCGGATCTCATTGATGCCTGGAGATCCTTACTC
HS315_MS2 pET F	TGTTTAACTTTAAGAAGGAGATATACCATGTTTCAGAATTCAAAAGATCTAGGAGGG
HS305_P22 AURW R	AGAACCACCACGCCAACGCCAACGCCAACGCATGATTAACTCTCTCTTATTGAGGTTG
HS304_P22 AURW F	CGCAGCAATGCCGTAGCA
HS303_P22 AUSE R	CCAAGCGAGGCACCCCACCATAATTTTTCCGACATGATTAACTCTCTCTTATTGAGGTTG
HS302_P22 AUSE F	TCGGAAAAATTATGGTGGGGTGCCTCGCTTGGTGGTTCTGGTCGCAGCAATGCCGTAGCA
HS301_P22 AG4 R	GATGGCAAATAACGGAAAAGACTAGACGGATTCATGATTAACTCTCTCTTATTGAGGTTG
HS300_P22 AG4 F	TCTAGTCTTTTCCGTTATTTGCCATCTGATGGTGGTTCTGGTCGCAGCAATGCCGTAGCA
HS299_P22 AGP35 F	TAGCCCTACGCCTCACGTCGTTACGGGTGGTTCTGGTCGCAGCAATGCCGTAGCA
HS298_P22 AGP35 R	ACGACGTGAGGCGTAGGGCTACGCCAGCTCCACATGATTAACTCTCTCTTATTGAGGTTG
HS297_MS2_AUSE R	AAGCGAGGCACCCCACCATAATTTTTCCGAGGCGGAGCTTTGACGAACAC
HS296_MS2_AUSE F	TCGGAAAAATTATGGTGGGGTGCCTCGCTTCAAAATCGTAAATACACCATTAAGGTGG
HS295_MS2_AURW R	ACGCCAACGCCAACGCCAACGGGAGCTTTGGGAGCTTTGACGAACACTACACG
HS294_MS2_AURW F	CGTTGGCGTTGGCGTTGGCGTGCCCAAAATGCCCAAAATCGTAAATACACCA
HS293_MS2_AGP35 R	CGTAACGACGTGAGGCGTAGGGCTACGCCAGCTCCAGGCGGAGCTTTGACGAACAC
HS292_MS2_AGP35 F	GCTGGCGTAGCCCTACGCCTCACGTCGTTACGCAAAATCGTAAATACACCATTAAGGTGG
HS291_MS2_AG4 R	ATCAGATGGCAAATAACGGAAAAGACTAGACGGATTGGAGCTTTGACGAACACTACACG
HS290_MS2_AG4 F	AATCCGTCTAGTCTTTTCCGTTATTTGCCATCTGATGCCCAAAATCGTAAATACACCA
HS289_MS2-wt R	TTGATGCCTGGAGATCCTTACTC
HS288_MS2-wt F	TTTCAGAATTCAAAAGATCTAGGAGGG
HS287_pET28_rseq	TAGTTATTGCTCAGCGGTGGC
HS286_pET28_fseq	TCTCGATCCCGCGAAATTAAT